PHYSICAL REVIEW B VOLUME 15, NUMBER 1 1 JANUARY 1977

Global phase diagram for a three-component model*

D. Furman, S. Dattagupta,† and Robert B. Griffiths
Physics Department, Carnegie-Mellon University, Pittsburgh, Pennsylvania 15213
(Received 12 April 1976)

The global phase diagram in a five-dimensional parameter space is described for a model which can be thought of as the "regular-solution" model of a ternary mixture or the mean-field approximation to a spin-1 Ising ferromagnet with a general nearest-neighbor interaction (the Blume-Capel model). The model possesses three fourth-order critical points (known from previous work) which are connected to a total of nine lines of tricritical points. Four manifolds of four-phase coexistence occur along with three manifolds of double critical points and six manifolds of critical double-end points. The locations of all significant features of the phase diagram are described qualitatively, and quantitative results are provided for some of the manifolds of lower dimension. Computational procedures are described which permit a detailed exploration of any portion of the phase diagram which may be of interest.

I. INTRODUCTION

In this paper we describe the entire global phase diagram for a model three-component system which has been the subject of a number of papers on phase transitions and higher-order critical points in complex systems. The model (defined in detail in Sec. II below) may be thought of in various ways: as the mean-field approximation to a spin-1 Ising magnet with the most general type of single-ion and exchange interactions, as a "regular mixture" of three components, as a model of phase separation in ternary alloys, as a model of a mixture of two compressible fluids, etc.

Our concern is not the physical applications of the model, but rather the mathematical structure of its phase diagram which may be thought of lying, in a rather natural sense, in a five-dimensional space of thermodynamic parameters (Sec. III). Previous authors[1-10] have described selected portions of this five dimensional space in greater or lesser detail. We, on the other hand, present an overall description of the phase diagram showing its qualitative behavior in all regions of the parameter space and providing quantitative information about some of the salient features.

Such a qualitative understanding of the phase diagram is of considerable importance in practical applications of the model. One can hardly expect the three-component model to provide detailed and correct quantitative information about any particular system, not only because the values of the parameters (in the model) appropriate to real systems are unknown, but also because the model is a considerable oversimplification of physical reality. Thus in particular the critical points in the model are "classical" and do not take proper account of statistical fluctuations. However, one might still expect it to yield correct qualitative features of phase diagrams of real systems, such as the connectivity of various coexistence and critical surfaces, in the same way that the mean-field model of a ferromagnet or the van der Waals model of a fluid yield phase diagrams with a coexistence line terminating in a critical point, in agreement with experiment. It may, of course, turn out that in some circumstances the three-component model unexpectedly gives qualitatively incorrect phase diagrams. This would itself be quite interesting and might indicate (for example) hitherto unobserved types of critical phenomena. Such a possibility provides yet another motivation for working out the qualitative features of the global phase diagram of the model in detail. Further remarks on the extent to which, and the manner in which, the three-component model phase diagrams may be expected to agree with experimental observations on real fluid mixtures and other systems are found in Sec. V.

The three-component model is in a certain sense (Sec. II B) a generalization of the mean-field approximation of the usual Ising model, or the corresponding lattice gas, to the next simplest situation. It is also closely analogous, though not identical, to a particular form of the van der Waals model for a binary mixture (Sec. II A). Indeed, a certain portion of the global phase diagram for this van der Waals model has been calculated previously by Scott and Van Konynenburg,[11] and our results show an important resemblance to (as well as significant differences from) the van der Waals case.

There are, of course, some practical difficulties in attempting to present an overall view of a phase diagram in a five-dimensional parameter space. Our approach is to focus attention on the features of highest codimension (in the notation of Ref. 12), such as tricritical points and points of four-phase

coexistence, which occur on smooth manifolds (surfaces) of relatively low dimensionality in the parameter space. The value of this approach is apparent from an analogy with the phase diagram of a pure substance, consisting of two-phase coexistence lines connecting various triple and critical points. Given only the locations of the triple and critical points (the features of highest codimension in this case), together with the knowledge of which points are connected to which, one would have a good qualitative understanding of the structure of the diagram, though not enough information to reconstruct it accurately in detail.

Our results are presented both numerically and in terms of graphs giving projections and sections of various parts of the phase diagram. The majority of the graphs employ "field" variables[13] in contrast to the mixture of "field" and "density" variables traditionally employed for multicomponent mixtures. The latter, while providing the most convenient representation of experimental data, make it difficult to separate intrinsic features of the global phase diagram from those which are "accidental" consequences of the choice of coordinates. It should be noted, however, that the numerical techniques which we (and others) have used to explore the global phase diagram also yield phase diagrams in the mixed variables used to describe experiments.

The earliest studies of the three-component model of which we are aware are the two papers[1] of Meijering which present a complete mathematical formulation of the problem and a number of phase diagrams. In a subsequent paper[2] Meijering noted all the important features in the symmetric section Σ_{ab} (our notation, Sec. II). Many of his results have been subsequently rediscovered by others. Various authors[3-6] have investigated the three-component model as a mean-field approximation to a spin-1 Ising magnet. We are indebted to Mukamel and Blume[7] and Krinsky and Mukamel[8,9] (the latter consider the analogous four-component model) for certain mathematical techniques. Recently Lajzerowicz and Sivardière[10] have discussed a number of applications of the three-component model (plus "antiferromagnetic" analogs not included in the three-component model as we define it) to a variety of physical systems and have calculated a number of phase diagrams. Omitted from the above listing (and our bibliography) are a large number of papers devoted to applications of the three-component model to various systems, but which do not contain any essentially new information on phase diagrams.

An outline of the remainder of this paper is as follows. The three-component model is defined and its relationship to mean-field theories is discussed in Sec. II. Table I presents a comparison of our notation with that of some previous investigators.

Section III is the heart of the paper. It begins (Sec. III A) with a discussion of the sections and projections used to present the global phase diagram, and the permutation symmetry which permits optimum use of the information presented subsequently. An overview (Sec. III B) of the global phase diagram is followed by a detailed qualitative discussion (Secs. III C and III D) of its various features, including a tabulation (Table II) of some of the entities occurring in different parts of the parameter space. A selection of numerical values for various prominent features of the phase diagram is presented in Table III. A discussion (Sec. III E) of topological properties of the phase diagram concludes this section. Some of the most important topological information is presented in Table IV, which gives a list of manifolds, apart from ordinary critical points, of dimension less than or equal to three (codimension two or greater).

Section IV (which should be omitted on a first reading) describes the mathematical procedures we have used to investigate the phase diagram. Certain unedifying details concerning tricritical points are consigned to the Appendix.

Finally, a brief discussion of some matters which should be kept in mind when comparing the three-component model with real systems is presented in Sec. V, concluding the paper.

II. THREE-COMPONENT MODEL

A. As a three-component mixture

Consider a ternary mixture or alloy containing N_x, N_y, and N_z moles of three different components, and

$$N = N_x + N_y + N_z \tag{2.1}$$

moles altogether. A phenomenological ("regular solution") model of this mixture is obtained by assuming the Gibbs potential G has the form

$$G = N[\hat{a}yz + \hat{b}xz + \hat{c}xy + RT(x \ln x + y \ln y + z \ln z)], \tag{2.2}$$

where $\hat{a}$, $\hat{b}$, and $\hat{c}$ are phenomenological "energy parameters" and $x = N_x/N$, y, and z are the mole fractions of the three components. It is convenient to divide this equation by NRT to obtain ($\overline{G} = G/NRT$):

$$\overline{G} = \overline{a}yz + \overline{b}xz + \overline{c}xy + x \ln x + y \ln y + z \ln z, \tag{2.3}$$

where

$$\overline{a} = \hat{a}/RT, \quad \overline{b} = \hat{b}/RT, \quad \overline{c} = \hat{c}/RT \tag{2.4}$$

will also be called energy parameters.

This model is said to show multiple-phase coexistence provided the minimum on the right-hand side of the equation

$$\pi(\nu_1, \nu_2) = \min_{x,y} (\overline{G} - \nu_1 x - \nu_2 y) \tag{2.5}$$

is achieved at more than one point in the triangle

$$x \geq 0, \quad y \geq 0, \quad x + y \leq 1 \tag{2.6}$$

for a suitable choice of ν_1 and ν_2. In taking the minimum in (2.5), z is to be replaced by $1-x-y$, since the sum of the mole fractions is one:

$$x + y + z = 1. \tag{2.7}$$

If the minimum is achieved at x_1, y_1 and x_2, y_2, we say that two phases with these compositions coexist, or that for this particular choice of the parameters $\overline{a}$, $\overline{b}$, $\overline{c}$, ν_1, and ν_2 there is two-phase coexistence. A geometrical interpretation is obtained by assuming the function $\overline{G}$ defines a curved surface over the x, y triangle (2.6). When two phases coexist, there is a plane tangent to the $\overline{G}$ surface at the two points in question. It has slopes ν_1 and ν_2 in the x and y directions, respectively, and lies below the $\overline{G}$ surface at all other points.

Likewise three or more phases are said to coexist if the minimum in (2.5) is achieved simultaneously (fixed ν_1 and ν_2) at three or more points or, equivalently, if there is a plane tangent to the $\overline{G}$ surface at the points in question and lying below it elsewhere. Strictly speaking, the *equilibrium* Gibbs potential divided by NRT is not $\overline{G}$, but its convex hull whose graph is obtained from that of $\overline{G}$ by replacing the curved surface with a straight line between pairs of coexisting phases, or a flat triangle between three coexisting phases, etc. Note that adding a constant or terms linear in x and y (or z) to the right side of (2.2) or (2.3) has no effect on phase coexistence apart from adding constants to the values of ν_1 and ν_2 (and π) at which it occurs.

In place of ν_1, ν_2, and π it is often convenient to use variables more obviously related to the permutation symmetry (Sec. III A) of the three-component model. The chemical potentials, defined by

$$\mu_x = \left(\frac{\partial G}{\partial N_x}\right)_{T,N_y,N_z} = RT\nu_x \tag{2.8}$$

and its analogs, are given explicitly by the formulas

$$\begin{aligned} \nu_x &= \overline{b}z + \overline{c}y + \ln x - w, \\ \nu_y &= \overline{a}z + \overline{c}x + \ln y - w, \\ \nu_z &= \overline{a}y + \overline{b}x + \ln z - w, \\ w &= \overline{a}yz + \overline{b}xz + \overline{c}xy. \end{aligned} \tag{2.9}$$

Equation (2.5) implies that

$$\begin{aligned} \nu_1 &= \nu_x - \nu_z, \\ \nu_2 &= \nu_y - \nu_z, \\ \pi &= \nu_z \end{aligned} \tag{2.10}$$

provided ν_x, ν_y, and ν_z are evaluated using (2.9) for x and y at the minimum (or any of the minima) of the right-hand side of Eq. (2.5).

For drawing phase diagrams (Sec. III), it is convenient to introduce the variables (closely related to activities)

$$\zeta_x = e^{\nu_x}/\zeta, \quad \zeta_y = e^{\nu_y}/\zeta, \quad \zeta_z = e^{\nu_z}/\zeta \tag{2.11}$$

with

$$\zeta = e^{\nu_x} + e^{\nu_y} + e^{\nu_z}. \tag{2.12}$$

An explicit formula for ζ_x is

$$\zeta_x = xe^{\overline{b}z+\overline{c}y}(xe^{\overline{b}z+\overline{c}y} + ye^{\overline{a}z+\overline{c}x} + ze^{\overline{b}x+\overline{a}y})^{-1}. \tag{2.13}$$

Multiplying (2.2) by a positive factor has no influence on phase coexistence. Consequently we have found it convenient, when discussing phase diagrams, to adopt a particular normalization for the energy parameters:

$$|\hat{a}| + |\hat{b}| + |\hat{c}| = 1, \tag{2.14}$$

which means [see (2.4)] that

$$RT = (|\overline{a}| + |\overline{b}| + |\overline{c}|)^{-1}. \tag{2.15}$$

We shall call the parameters $\overline{a}$, $\overline{b}$, $\overline{c}$, ν_1, ν_2, and π "field variables" or "fields" (in contrast to the "density" variables x, y, and z) because they are always identical in two or more coexisting phases.[13] Likewise ν_x, ν_y, and ν_z, and ζ_x, ζ_y, and ζ_z are fields. By varying one or more fields it is possible to make two coexisting phases move closer together until they coalesce to form a critical point, which we denote[12] by B. Likewise if there are three coexisting phases, denoted by AAA or A^3, the fields may be altered so that two of them coalesce while coexisting with the third to form a critical end point BA. Or the three phases may simultaneously coalesce at a tricritical point C. Other possibilities arise if various points associated with four-phase coexistence A^4 are allowed to coalesce[14]: a critical point coexisting with two phases BA^2, two coexisting critical points or a "double critical point" B^2, a tricritical end point CA, and a fourth-order critical point D.

The mathematical form (2.2) is closely related to the Helmholtz free energy for the van der Waals model of a binary mixture with constant b parameter and the a parameter a quadratic function of composition.[11] However, N is to be interpreted as the volume, x and y as the numbers of molecules of types 1 and 2 per unit volume divided by their

maximum values, and $z \ln z$ in (2.2) is to be replaced by $(z-1)\ln z$. If $z \ln z$ is left unchanged, (2.2) may (with the above interpretation) be thought of as a phenomenological model of a binary mixture, though with somewhat different properties from the van der Waals model.

B. As the mean-field approximation for a three-component lattice "gas"

We suppose that the volume occupied by the "gas" is divided into cells whose centers form a regular lattice. Each cell contains one and only one molecule, which may be of type 1, 2, or 3. If the jth cell contains a molecule of type α, $P_j^{(\alpha)}$ is equal to 1, and otherwise it is zero. We suppose the energy is of the form[8]

$$\mathcal{H} = -q^{-1} \sum_{\alpha} \sum_{\beta} E_{\alpha\beta} \sum_{\langle ij \rangle} P_i^{(\alpha)} P_j^{(\beta)} - \sum_{\alpha} \mu_\alpha \sum_i P_i^{(\alpha)}, \tag{2.16}$$

where q is the coordination number of the lattice, $E_{\alpha\beta} = E_{\beta\alpha}$ is minus the energy of interaction if molecules of type α and β are in nearest-neighbor cells, and $\langle ij \rangle$ denotes a pair of nearest-neighbor cells with each pair included in the sum only once. In the mean-field approximation the free energy F for a system with $\bar{N}$ cells is given by[8]

$$F/\bar{N} = kT \sum_{\alpha} A_\alpha \ln A_\alpha - \frac{1}{2} \sum_{\alpha} \sum_{\beta} E_{\alpha\beta} A_\alpha A_\beta - \sum_{\alpha} \mu_\alpha A_\alpha, \tag{2.17}$$

where k is Boltzmann's constant and

$$A_\alpha = \langle P_j^{(\alpha)} \rangle, \tag{2.18}$$

the thermal average of $P_j^{(\alpha)}$ or the probability that the jth cell is occupied by a molecule of type α, is assumed to be independent of j. We shall not consider cases where $\langle P_j^{(\alpha)} \rangle$ depends on j. Upon making the identifications

$$x = A_1, \quad y = A_2, \quad z = A_3; \tag{2.19}$$

$$\bar{\nu}_x = (\mu_1 + \tfrac{1}{2}E_{11})/kT,$$
$$\bar{\nu}_y = (\mu_2 + \tfrac{1}{2}E_{22})/kT, \tag{2.20}$$
$$\bar{\nu}_z = (\mu_3 + \tfrac{1}{2}E_{33})/kT;$$

$$\bar{a} = \tfrac{1}{2}(E_{22} + E_{33} - 2E_{23})/kT,$$
$$\bar{b} = \tfrac{1}{2}(E_{11} + E_{33} - 2E_{13})/kT, \tag{2.21}$$
$$\bar{c} = \tfrac{1}{2}(E_{11} + E_{22} - 2E_{12})/kT;$$

it can be shown that

$$\bar{G} - x\bar{\nu}_x - y\bar{\nu}_y - z\bar{\nu}_z = F/\bar{N}kT. \tag{2.22}$$

Mean-field theory requires that $F/\bar{N}kT$ be minimized with respect to the A_α with the μ_α and $E_{\alpha\beta}$ held fixed,

$$\psi = \min_{\{A_\alpha\}} (F/\bar{N}kT). \tag{2.23}$$

This is obviously equivalent to minimizing the left-hand side of (2.22) at fixed $\bar{\nu}_x$, $\bar{\nu}_y$, $\bar{\nu}_z$, $\bar{a}$, $\bar{b}$, and $\bar{c}$, which in turn is equivalent to (2.5) with the identification

$$\nu_1 = \bar{\nu}_x - \bar{\nu}_z,$$
$$\nu_2 = \bar{\nu}_y - \bar{\nu}_z, \tag{2.24}$$
$$\pi = \psi + \bar{\nu}_z.$$

Combining (2.10) and (2.24) one obtains, at the minimum

$$\psi = \nu_x - \bar{\nu}_x = \nu_y - \bar{\nu}_y = \nu_z - \bar{\nu}_z. \tag{2.25}$$

In such a lattice-gas model it is always possible to regard one of the components, say $\alpha = 3$, as "vacuum", in which case one has a crude model of a compressible binary mixture in which each cell may be vacant or occupied by at most one molecule of type 1 or 2.

C. As the mean-field approximation for a spin-1 Ising magnet

The spin variable S_j on the jth site of a lattice can take on the values 0, 1, and -1, and the energy is assumed to be

$$\mathcal{H} = -q^{-1}J \sum_{\langle ij \rangle} S_i S_j - q^{-1}K \sum_{\langle ij \rangle} S_i^2 S_j^2 - q^{-1}C \sum_{\langle ij \rangle} (S_i^2 S_j + S_i S_j^2) - H \sum_i S_i + \Delta \sum_i S_i^2. \tag{2.26}$$

The first two terms on the right-hand side describe nearest-neighbor dipolar and quadrupolar exchange, while H is a magnetic field (in suitable units) and Δ a crystal-field splitting. The term C is normally absent in magnetic systems, but is introduced here to allow for the most general mathematical form of nearest-neighbor interaction.

By expressing the S_j in terms of the $P_j^{(\alpha)}$ introduced above through

$$S_j = P_j^{(1)} - P_j^{(2)}, \tag{2.27}$$

and noting that ($\delta_{\alpha\beta}$ is the Kronecker δ)

$$P_j^{(\alpha)} P_j^{(\beta)} = P_j^{(\alpha)} \delta_{\alpha\beta}, \tag{2.28}$$

one can rewrite (2.26) in the form (2.16), and the mean-field approximation for the latter applies, with appropriate changes of notation, to the former. Note that we are *not* considering the possibility that $\langle S_j \rangle$ may depend on the site j; i.e., we are deliberately excluding the possibility of antifer-

TABLE I. Comparison of notation with that of some previous authors.

This paper	Meijering [a]	Capel [b]	Mukamel and Blume [c]	Mukamel and Krinsky [d]	Sivardière and Lajzerowicz [e]
$\bar{a}$	γ	$\frac{1}{2}\alpha$	$(J+K-2C)/2kT$	$(E_0+E_2)/2kT$	$(J+K-2L)/2kT$
$\bar{b}$	β	$\frac{1}{2}\alpha$	$(J+K+2C)/2kT$	$(E_0+E_1)/2kT$	$(J+K+2L)/2kT$
$\bar{c}$	α	2α	$2J/kT$	$(E_1+E_2)/2kT$	$2J/kT$
ν_1 [f]	$(\mu_x-\mu_z)/RT$	$\alpha(1/2+\beta-\gamma)$	$\bar{b}-(\Delta-H)/kT$	$\bar{b}+\mu_3/kT$	$\bar{b}+(D+H)/kT$
ν_2	$(\mu_y-\mu_z)/RT$	$\alpha(1/2-\beta-\gamma)$	$\bar{a}-(\Delta+H)/kT$	$\bar{a}+\mu_1/kT$	$\bar{a}+(D-H)/kT$
ν_z	μ_z/RT	F/NkT	ϕ/NkT	ϕ/kT	ϕ/kT
x	x	$\frac{1}{2}(1+\sigma-\rho)$	$\frac{1}{2}(Q+M)$	A_1	$x_A=\frac{1}{2}(Q+M)$
y	y	$\frac{1}{2}(1-\sigma-\rho)$	$\frac{1}{2}(Q-M)$	A_3	$x_C=\frac{1}{2}(Q-M)$
z	z	ρ	$1-Q$	A_0	$x_B=1-Q$

[a] Reference 1.
[b] Reference 4. Note that only the case $\bar{a}=\bar{b}=\frac{1}{4}\bar{c}$ is considered.
[c] Reference 7.
[d] Reference 8 with $A_2=0$, $\mu_2=-\infty$
[e] Reference 10.
[f] Note that $\nu_x=\nu_1+\nu_z$ and $\nu_y=\nu_2+\nu_z$

romagnetism. The relationship between the constants in (2.26) and those in Sec. II A above is shown in Table I.

III. GLOBAL PHASE DIAGRAM

A. Sections, projections, and symmetries

One can think of the global phase diagram of the three-component model as a set of manifolds or curved (hyper)surfaces representing A^2, B, etc., of appropriate dimensionality in the five-dimensional field space spanned by $\bar{a}$, $\bar{b}$, $\bar{c}$, ν_1, and ν_2. It is convenient to describe the global diagram in terms of its *projections* onto spaces of lower dimensionality and in terms of *sections* of the complete diagram obtained by holding some of the field variables constant. We shall not employ any sections obtained by holding a density variable fixed, but the diagram for the section itself may be drawn using either field or density variables.

The section obtained by holding $\hat{a}$, $\hat{b}$, and $\hat{c}$ fixed will be called a *system* phase diagram, because in the simplest physical interpretation of the three-component model as a liquid mixture these quantities represent molecular properties which are fixed by the nature of the system under study, while the remaining variables in (2.2), the compositions and the temperature, can be altered in the laboratory. (See Sec. V, however, for additional remarks on the relationship of this model to real mixtures.)

Two systems in which $\hat{a}$, $\hat{b}$, and $\hat{c}$ have the same ratios and the same signs give rise to identical system phase diagrams apart from a scaling factor for the temperature. Consequently, we will always assume that the magnitudes of $\hat{a}$, $\hat{b}$, and $\hat{c}$ sum to unity, (2.14), and the temperature is determined by $\bar{a}$, $\bar{b}$, and $\bar{c}$ in accordance with (2.15)

A two-dimensional section at fixed $\bar{a}$, $\bar{b}$, and $\bar{c}$, or equivalently fixed $\hat{a}$, $\hat{b}$, $\hat{c}$, and T, can be either a composition or activity triangle. The former, of which Fig. 1(a) is an example, is an equilateral triangle with composition represented in barycentric coordinates: a point inside the triangle is at the center of mass if masses of magnitude x, y, and z $(=1-x-y)$ are placed at the corresponding vertices. The latter is also an equilateral triangle, Fig. 1(b), but the masses for the barycentric coordinates are now ζ_x, ζ_y, and ζ_z $(=1-\zeta_x-\zeta_y)$ as defined in (2.11).

In the composition triangle the edge opposite to the z vertex, along which $z=0$, represents the binary system in which the third component (mole fraction z) is absent. The same is true of the edge opposite ζ_z in the activity triangle, since μ_z or ν_z

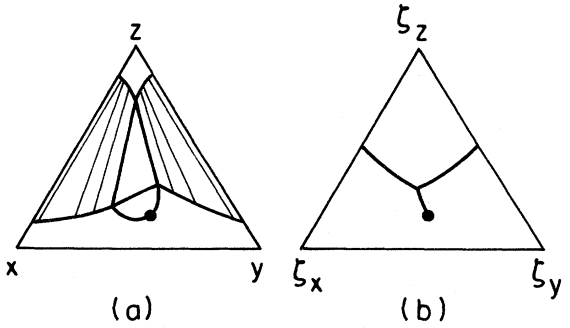

FIG. 1. (a) Phase diagram in the composition triangle; (b) the corresponding diagram in the activity triangle.

is $-\infty$ in a system in which $z=0$. Likewise the vertices in both the composition and activity triangles represent the corresponding pure components. However, in other respects the composition and activity triangles are quite different. Because the latter is spanned by field variables, two-phase coexistence is represented by single lines and three-phase coexistence by points, in contrast to two-phase regions and three-phase triangles in the former. Figures 1(a) and 1(b) represent the same physical situation. With a little practice it is not difficult to construct a phase diagram in the activity triangle which represents qualitatively the same behavior (i.e., the correct topological features) as a given diagram in the activity triangle, and vice versa.

A system phase diagram in a triangular prism with the temperature axis vertical and an activity triangle as the base is shown in Fig. 2(a). There are two coexistence surfaces Σ_1 and Σ_2 terminating on lines of critical points σ_1 and σ_2. The surfaces intersect in a triple line τ, which in turn joins σ_1 at a critical end point. A section of Fig. 2(a) at an appropriate constant temperature yields the diagram in Fig. 1(b).

Since it is tedious to draw three-dimensional diagrams in perspective, it is sometimes useful to project the principal features of a system diagram along the temperature axis onto the triangular base. Figure 2(b) is a projection of the critical lines in Fig. 2(a). Once again, a little practice makes it possible in many cases to reconstruct the essential topological features of a system phase diagram given a projection as in Fig. 2(b).

The projection along ν_1 and ν_2 onto the three-dimensional "energy space" spanned by $\bar{a}$, $\bar{b}$, and $\bar{c}$ (which we refer to, somewhat inaccurately, as "energy parameters") plays an important role in our description of the global phase diagram. One can think of this projection in the following way. If a particular feature of interest, such as C or A[4], occurs somewhere in the composition (or activity) triangle for a given choice of $\bar{a}$, $\bar{b}$, and $\bar{c}$, then the corresponding point in the energy space is assigned an appropriate color. Points of one color then form zero-, one-, two-, or three-dimensional manifolds in the energy space, and one has a projection of certain salient features of the global phase diagram onto a space of lower dimensionality.

Due to limitations of graphical presentation, it is in addition convenient to project the different octants of the energy space onto a set of eight "energy triangles" in the following manner. For the octant $\bar{a}\geq 0$, $\bar{b}\geq 0$, $\bar{c}\geq 0$, we use a barycentric representation on an equilateral triangle, Fig. 3(a), with weights equal to $\hat{a}$, $\hat{b}$, and $\hat{c}$ at the vertices. We shall call this the principal energy triangle. For the octant with $\bar{a}<0$, $\bar{b}\geq 0$, $\bar{c}\geq 0$, the corresponding triangle has weights of $-\hat{a}$, $\hat{b}$, and $\hat{c}$ at the vertices. This triangle is drawn adjacent to and to the right of the principal triangle in Fig. 4, which also shows triangles corresponding to all the other octants. As a practical necessity, only a few features of the global phase diagram are indicated explicitly in Figs. 3 and 4, but from these it is possible to form a fair idea of the overall topological structure of the diagram, as we shall show. We shall sometimes consider an energy triangle as the base of a prism with vertical axis equal to the temperature. This provides another three-dimensional representation of the corresponding octant in the energy space.

The reason for employing equilateral triangles and the corresponding prisms for phase diagrams of the three-component model is that they exhibit, in a convenient way, an important symmetry of the model. Any permutation of $\bar{a}$, $\bar{b}$, $\bar{c}$ accompanied by the corresponding permutation of x, y, z leaves $\bar{G}$ in (2.3) unchanged. Thus the global phase

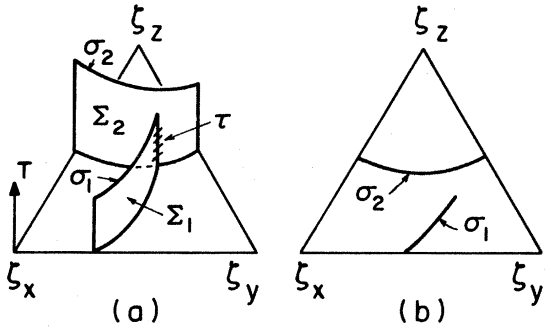

FIG. 2. System phase diagram in a triangular prism; (b) the critical lines in this diagram projected onto the base of the prism.

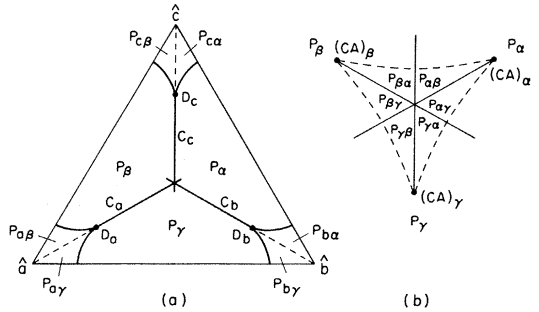

FIG. 3. Projection of the global phase diagram showing (a) the principal energy triangle and (b) the center of the triangle on an expanded scale.

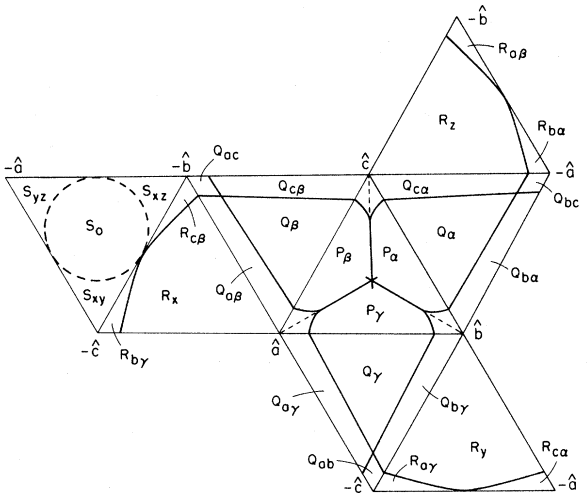

FIG. 4. Projection of the complete global phase diagram on the eight energy triangles.

diagram is unchanged provided $\bar{a}$, $\bar{b}$, $\bar{c}$ undergo some permutation and ζ_x, ζ_y, ζ_z or x, y, z simultaneously undergo a corresponding permutation. For example, if a particular feature, such as a tricritical point, occurs at $\bar{a}=\alpha_1$, $\bar{b}=\alpha_2$, $\bar{c}=\alpha_3$ and $\zeta_x=\beta_1$, $\zeta_y=\beta_2$, $\zeta_z=\beta_3$ $(=1-\beta_1-\beta_2)$, the same feature will also occur at $\bar{a}=\alpha_2$, $\bar{b}=\alpha_3$, $\bar{c}=\alpha_1$, $\zeta_x=\beta_2$, $\zeta_y=\beta_3$, $\zeta_z=\beta_1$. This symmetry is clearly evident in Figs. 3 and 4, and greatly simplifies the task of describing the global phase diagram.

The global phase diagram also possesses certain symmetrical sections which are carried into themselves by certain of the permutations just discussed. The one-dimensional symmetry axis $\bar{a}=\bar{b}=\bar{c}$, $\zeta_x=\zeta_y=\zeta_z=\frac{1}{3}$ is carried into itself by all permutations. The three-dimensional section Σ_{ab} obtained by setting $\bar{a}=\bar{b}$ and $\zeta_x=\zeta_y$ is invariant under the simultaneous interchange of $\bar{a}$ with $\bar{b}$ and ζ_x and ζ_y. The sections Σ_{ac} and Σ_{bc} are defined in analogy with Σ_{ab}.

B. Overview of the global phase diagram

Figure 4 shows a projection of certain prominent features of the full five-dimensional phase diagram on the set of eight energy triangles defined in Sec. III A above. These triangles together form an octahedron with a threefold rotation axis passing through the centers of the P (principal) and S triangles. Note that the edges with identical labels are the same on the octahedron, and hence (for example) the regions marked Q_{ab} and $R_{b\gamma}$ should be thought of as adjacent to each other along the edge $\hat{a}$, $-\hat{c}$, even though they appear separated in the figure. An enlarged diagram of the principal energy triangle $\hat{a}$, $\hat{b}$, $\hat{c}$ appears in Fig. 3(a), and Fig. 3(b) shows the region near the center of this triangle further enlarged.

The solid lines which are not sides of energy triangles in Figs. 3 and 4 are projections of lines of C or tricritical points. Three lines of tricritical points come together at each of the fourth-order critical points labeled D (with a subscript) in Fig. 3. Elsewhere these C lines do not intersect each other even though they appear to do so in the projection (as, for example, at the center of the principal triangle.)

The dashed lines in the principal triangle represent boundaries of manifolds of four-phase coexistence, which will be discussed in greater detail below. The dashed circle in the S triangle and the straight lines which form the edges of the energy triangles represent points where certain characteristic features of the phase diagram go to zero temperature.

The solid and the dashed lines in Figs. 3 and 4 together divide the eight energy triangles into 40 two-dimensional regions, with the property that within each region the corresponding system phase diagrams are all topologically similar: i.e., the connection of various coexistence surfaces and the presence or absence of critical end points of various types is the same for all system diagrams. This means that a complete qualitative description of the global phase diagram is available once descriptions of the diagrams are provided for each of these 40 regions. The regions are labeled using a capital letter to indicate how many of the energy parameters are positive (three for P, two for Q, one for R, and zero for S), and subscripts which are related, as we shall see, to certain characteristics of the corresponding system diagrams. The subscripts are chosen so that different regions related by a symmetry of the phase diagram are labeled by corresponding subscripts, with greek subscripts α, β, γ to be permuted in the same manner (and simultaneously with) a, b, c and x, y, z. When the permutation symmetry is taken into account, one finds that there are only ten distinct types of two-dimensional regions in the energy triangles. These are listed in Table II, together with some of the features which occur in each region. Naturally, a complete specification of the global phase diagram also requires a knowledge of the system diagrams for points lying on the dividing lines between the two-dimensional regions, and the points where these lines come together. We shall include this information in our discussion.

System diagrams for various points, which we shall call "energy points," in the principal energy triangle are given in Sec. III C below, and for the other energy triangles in Sec. III D. We use symbols such as ○, ✕, etc., to indicate points in an

TABLE II. Entities occurring in different system phase diagrams. A representative example of each of the regions in Figs. 3 and 4 is listed in the first column followed by the number s of regions equivalent to it under permutation symmetry. The third column lists a figure or figures showing a "typical" system phase diagram and the fourth column lists each type of entity which occurs in this diagram with a subscript to indicate the manifold to which it belongs.

Region	s	Figure	Entities in diagram [a]
P_β	3	5(b), 5(c), 5(e)	$(A^3)_I$, $(BA)_\beta$
$P_{\gamma\alpha}$	6	6(b), 6(c)	$(A^3)_I$, $(A^4)_I$, $(BA)_\gamma$
			$(BA)_\gamma$, $(BA)_\alpha$
$P_{c\beta}$	6	10(c)	$(A^3)_I$, $(A^3)_{c\beta}$, $(BA)_\beta$
			$(BA)_{c\beta}$, $(BA)_{\beta c}$
Q_β	3	12(b)	
$Q_{c\beta}$	6	12(c)	$(A^3)_{c\beta}$, $(BA)_{c\beta}$, $(BA)_{\beta c}$
$Q_{ac}=Q_{ca}$	3	12(e)	$(A^3)_{c\beta}$, $(BA)_{c\beta}$, $(BA)_{\beta c}$
			$(A^3)_{a\beta}$, $(BA)_{a\beta}$, $(BA)_{\beta a}$
R_x	3	13(b)	
$R_{c\beta}$	6	13(c)	$(A^3)_{c\beta}$, $(BA)_{c\beta}$, $(BA)_{\beta c}$
$S_{xz}=S_{zx}$	3	13(e)	
S_0	1		

[a] A^2 and B occur in all regions except S_0, and have been omitted from the table.

energy triangle, and the same symbols are placed adjacent to the system diagrams. *Except where otherwise noted, the system phase diagrams and their projections are schematic and not numerically accurate.* Most of the features of interest in the phase diagram must be obtained numerically and cannot be expressed using simple formulas. Values of the parameters for some of the points of interest are shown in Table III.

C. Principal energy triangle

1. Regions with one critical end point

Figure 5 shows a set of system phase diagrams associated with points, hereafter called "energy points," in the principal energy triangle as indicated in Fig. 5(a). Figures 5(b) and 5(c) show diagrams associated with the energy point +. The former is analogous to Fig. 2(a) and shows a prism with the temperature axis vertical and the base of the prism at $T=0$, while the latter shows the projection of the critical lines onto the base of the prism, i.e., the activity triangle. Although Fig. 5(c) does not show the triple line or the coexistence surfaces, it gives a convenient summary of the information in Fig. 5(b) and is much easier to draw.

The energy point ○ in Fig. 5(a) is obtained from + by interchanging $\hat{a}$ and $\hat{b}$, and the system phase diagram can be obtained from Fig. 5(b) or 5(c) by the reflection corresponding to the interchange of ζ_x and ζ_y. It is shown in Fig. 5(d), the mirror image of Fig. 5(c). Likewise the energy point X arises from + by interchanging $\hat{a}$ and $\hat{c}$ or from ○ by a 120° counterclockwise rotation of Fig. 5(a), and its system diagram, shown in Fig. 5(e), is obtained from those of + or ○ by the corresponding reflection or rotation. It is thus evident that a proper use of symmetry reduces considerably the effort required to describe the system phase diagrams corresponding to different energy points.

Note that Figs. 5(c) and 5(e), although distinct, have the same general topological features. That is, one can be obtained from the other by continuous deformation without changing the fact that, for example, there is only one critical end point and it is connected by a critical line to the $\zeta_x\zeta_z$ side of the prism and by a triple line to $T=0$. Such critical end points will be said to be of β-type (since the $\zeta_x\zeta_z$ side is opposite the ζ_y edge of the prism, and we shall let α, β, and γ correspond to x, y, and z or a, b, and c). Critical end points of β-type form a smooth two-dimensional surface or manifold in the global phase diagram in a field space, and we shall denote it by $(BA)_\beta$.

All energy points in the (interior of the) region P_β in Fig. 3 give rise to system phase diagrams with the same general topological features shown in Fig. 5(b), and, in particular, possess a single β-type critical end point. However, as we shall see, the manifold $(BA)_\beta$ actually extends outside the P_β region. By symmetry, analogous remarks apply to the regions P_α and P_γ, and to the manifolds $(BA)_\alpha$ and $(BA)_\gamma$.

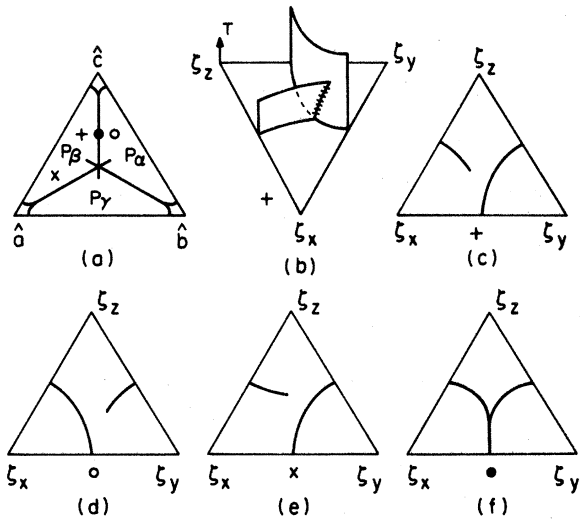

FIG. 5. System phase diagrams corresponding to the energy points shown in the principal triangle in (a) are shown schematically in (b)–(f).

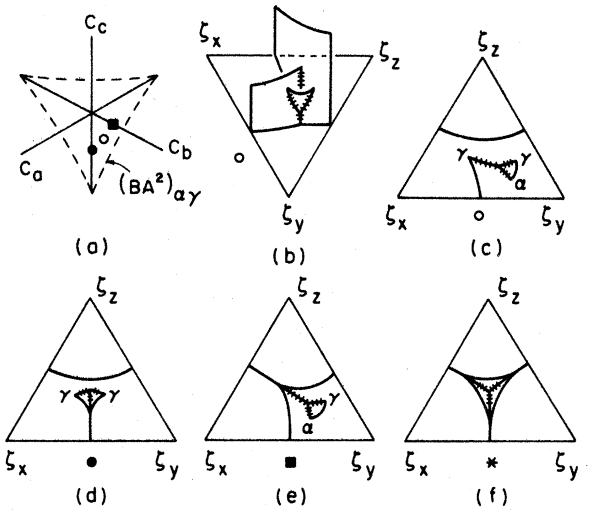

FIG. 6. System phase diagrams (schematic) in the "shield" region near the center of the principal triangle; (f) corresponds to the center of the shield.

2. *Tricritical points in symmetrical sections*

The energy point ● on the line separating P_α and P_β in Fig. 5(a) gives rise to the symmetrical diagram 5(f) with the critical lines from the three sides of the triangle all meeting at a tricritical point. This point evidently falls in the symmetric section Σ_{ab} (see Sec. III A above). It lies on a line or one-dimensional manifold of tricritical points which we label C_c and which extends all the way from the D_c point in Fig. 3(a) to the tricritical end point $(CA)_\gamma$ in Fig. 3(b). The equation for this manifold is found in Table III.

3. *"Shield" region*

The dashed curves in Fig. 3(b), which are approximately in the form of a hypocycloid, enclose a region which we shall call the "shield." For any energy point in the interior of the shield, the corresponding system phase diagram contains a point of four-phase coexistence A^4, which we shall call "type I" in distinction to "type II" discussed below. Some representative cases are shown in Fig. 6. The system phase diagram for ○ is shown in perspective in Fig. 6(b). This diagram is constructed by starting with one in which a single critical end point of type γ terminates a triple line from $T=0$ [analogous to Fig. 5(b)], and adding a small wedged-shaped piece of coexistence surface which touches the original triple line at a point of four-phase coexistence A^4 between $T=0$ and the critical end point. This wedge is itself joined to the other coexistence surfaces at triple lines, so that a total of four such lines meet at the A^4 point.

The same system diagram is shown in projection in Fig. 6(c), but with the triple line which goes to $T=0$ omitted [as is also the case in Figs. 6(d), 6(e), and 6(f)] in the interest of simplicity. Three critical end points, where a critical and triple line meet, occur in this diagram: two of type γ and one of type α, as indicated by the labeling. As only one of these is connected by a critical line to one side of the triangle and none of them is connected (directly) to the triple line which goes to $T=0$, some justification of this labeling is necessary, and it can be carried out by considering what happens to the system phase diagram as the corresponding energy point moves continuously.

Suppose that ○ in Fig. 6(a) is moved down and to the right until it crosses the dashed curve. The result is that the wedge-shaped coexistence surface in Fig. 6(b) or 6(c) shrinks in size until it vanishes. This vanishing corresponds to a BA^2 point, and, indeed, the dashed curves in Figs. 3(b) and 6(a) are projections of three manifolds of BA^2 points. [The one under discussion will be called $(BA^2)_{\alpha\gamma}$ or $(BA^2)_{\gamma\alpha}$, since it occurs on the boundary of both the $(BA)_\alpha$ and $(BA)_\gamma$. Note that it extends continuously from the $(CA)_\alpha$ to the $(CA)_\gamma$ point in Fig. 3(b).] The left-most critical end point in Fig. 6(c) is, however, unaffected by the shrinking of the wedge-shaped coexistence surface; and when the ○ has passed from the shield into the P_γ region, this critical end point still remains and is, obviously, of the type γ (the only type which occurs in the P_γ region). Thus, the left-most critical end point in Fig. 6(c) lies on the same manifold as the

other γ-type points, which justifies the label in the figure.

To identify the upper right-most critical end point in Fig. 6(c), consider what happens to the system phase diagram as ○ in Fig. 6(a) moves to the left to the C_c line, resulting in the diagram in Fig. 6(d), then to the left of this line, yielding a diagram which is qualitatively the mirror image, ζ_x exchanged with ζ_y, of Fig. 6(c), and finally further left into the P_γ region. During this process the upper right-most critical end point in Fig. 6(c) remains unaffected and hence, as it is still present at the end of this process, must of type γ.

Finally, to identify the remaining critical end point labeled α in Fig. 6(c), consider what happens if ○ in Fig. 6(a) is moved to the right and upwards till it meets the C_b line, yielding a diagram shown in Fig. 6(e). This diagram is symmetric under the interchange of ζ_x and ζ_z, which also interchanges the two critical end points. Thus if one of the critical end points is of type γ, as established by continuity in considering how Fig. 6(c) is transformed into Fig. 6(e), the other must be of type α by symmetry (since the permutation of x and z corresponds to the permutation of a with c and α with γ). An alternative argument can be constructed using a further displacement of the energy point from the position indicated by a solid square in Fig. 6(a) to the right into the region P_α, and checking that it is indeed the critical end point labeled α in Figs. 6(c) and 6(e) which remains at the end of this process.

The occurrence of two γ and one α critical end points in Fig. 6(c) is what suggests the terminology $P_{\gamma\alpha}$ for the corresponding region in Fig. 3(b). No doubt $P_{\gamma\gamma\alpha}$ would be a more explicit terminology, but $P_{\gamma\alpha}$ will suffice if one remembers that it is distinct from $P_{\alpha\gamma}$.

When the energy point is in the precise center of the principal triangle, the system phase diagram, shown in projection in Fig. 6(f), has three tricritical points. Since these occur at different points in the activity triangle (though, by symmetry, they all occur at the same temperature) it is plain, as we have remarked previously, that the tricritical point manifolds C_a, C_b, and C_c do not actually intersect in the full five-dimensional space, though they appear to do so when projected on the principal energy triangle.

If the solid square in Fig. 6(a) is moved along the C_b line away from the center of the diagram, the wedge-shaped region in the corresponding system phase diagram Fig. 6(e) shrinks until it eventually vanishes at an $\alpha\gamma$-type BA^2, just as the energy point in Fig. 6(a) crosses the dashed curve. This BA^2 point occurs both at a different temperature and at different activities than the tricritical point

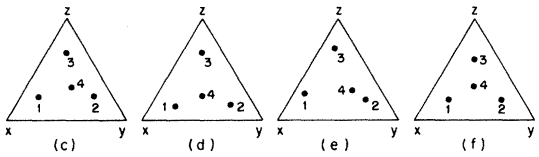

FIG. 7. Four-phase coexistence (schematic) in the composition triangle corresponding to the systems diagrams in Fig. 6. The labeling (c), (d), etc., corresponds to that in Fig. 6.

in the same system phase diagram, and thus the $(BA^2)_{\alpha\gamma}$ and C_b manifolds do not intersect in the full five-dimensional space.

The positions of the four coexisting phases in the composition triangle for the A^4 points in Fig. 6 are indicated in the corresponding parts of Fig. 7. The dot indicates the composition and the adjacent numbers serve to identify which phases correspond in the different figures. The phase four always lies inside the triangle formed by phases one, two, and three. At a $(BA^2)_{\alpha\gamma}$ point phases four and two coalesce, while at the $(CA)_\gamma$ point phase four, one, and two coalesce. The four-phase coexistence points form a single continuous manifold in the five-dimensional field space and the identity of the separate phases is always preserved (e.g., it is not possible to interchange phases two and three, or two and four, while remaining on the A^4 manifold).

4. Four-phase coexistence regions of type II

Regions of type-II four phase coexistence are indicated by the dashed lines terminating at the vertices of the principal energy triangle in Figs. 3 and 4. Since the projection on the energy triangle is not too enlightening, we show in Fig. 8 the portion of the symmetrical section Σ_{ab} ($\hat{a}=\hat{b}$) of the phase diagram with $\hat{a}$, $\hat{b}$, $\hat{c}$ positive, projected on a $\hat{c}$-temperature plane. It is helpful in interpreting this diagram to note that the two-dimensional manifold of type-II four-phase coexistence, labeled $(A^4)_c$, along with its boundaries $(B^2)_c$ and $(BA^2)_c$, projects onto the dashed line terminating at the $\hat{c}$ vertex of the principal triangle in Fig. 3. Hence, although in the full diagram the $(A^4)_{\mathrm{I}}$ and $(A^4)_{\mathrm{II}}$ manifolds have the same dimensionality, two, the latter, because it lies in a symmetrical section, has a lower-dimensional projection in the energy triangle. Similarly, unlike the $(A^4)_{\mathrm{I}}$ points, for a given choice of $\hat{a}=\hat{b}$ and $\hat{c}$, the A^4 points of type II persist over a finite temperature range, a "violation" of the phase rule noted by Meijering.[1]

The aforementioned symmetry also appears when the four coexisting phases are plotted in a compo-

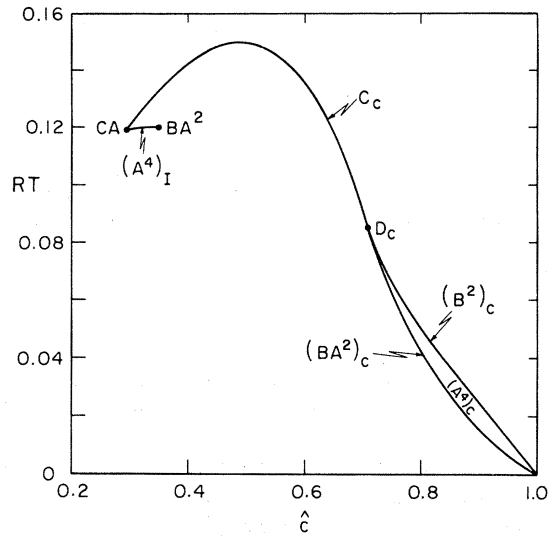

FIG. 8. Phase diagram in the Σ_{ab} section projected on the T, $\hat{c}$ plane. This drawing is to scale.

sition space, Fig. 9(a): phase two and four are mirror images of one and three, respectively, if x and y are interchanged. For fixed $\hat{a}=\hat{b}$ and $\hat{c}$, increasing temperature leads to one and three coalescing at the same point where two and four coalesce, giving rise to a double critical point B^2. The location of the B^2 points may be expressed by means of a parametric formula given below in Sec. IV, (4.27). With decreasing temperature, three and four coalesce at a BA^2 point. By varying $\hat{c}$ and the temperature, all four phases may be made to coalesce at the fourth-order point D_c. The system phase diagram which contains this fourth-order point is qualitatively similar to Fig. 5(f) and the fourth-order point occurs where the three critical lines come together. Its location is specified in Table III.

5. *Regions adjacent to four-phase coexistence of type II*

System phase diagrams for the regions adjacent to the vertices and inside the principal energy triangle are particularly difficult to represent in pro-

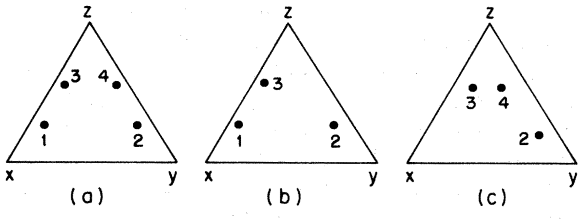

FIG. 9. Four-phase and three-phase coexistence (schematic) in the composition triangle.

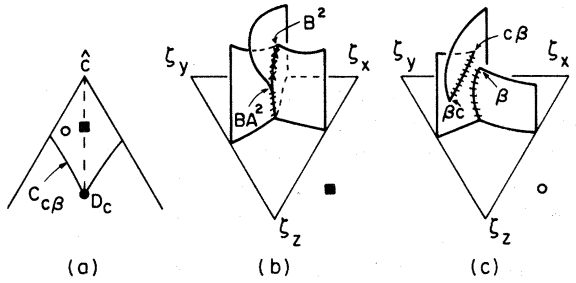

FIG. 10. System phase diagrams (schematic) near the $\hat{c}$ vertex of the principal energy triangle.

jection, so Fig. 10 shows schematic drawings in perspective. Figure 10(b) is a system phase diagram for $\hat{a}=\hat{b}$, indicated by the solid square in Fig. 10(a). At low temperatures there is a three-phase line terminating coexistence surfaces emanating from the three sides of the prism. However, at a certain temperature a BA^2 point occurs and the surfaces from the $\zeta_x\zeta_z$ and $\zeta_y\zeta_z$ sides begin to "cut in" to the third surface along a line (marked with X's) of four-phase coexistence which eventually terminates at a B^2 point. The critical line emanating from the BA^2 point arches over the B^2 point and terminates on the $\zeta_x\zeta_y$ side of the prism. Note that the diagram is invariant under the interchange of ζ_x and ζ_y.

If the energy point in Fig. 10(a) is moved to the left, to the point shown as ○, the result is the system diagram shown in Fig. 10(c). The B^2 point in Fig. 10(b) has split into two critical end points labeled β and $c\beta$, and the BA^2 point has become a critical end point βc. The A^4 line has disappeared and instead one finds one A^3 line extending to $T=0$ from the β-type BA point, and another extending between the $c\beta$ and βc BA points.

If, in turn, the ○ in Fig. 10(a) is allowed to move downwards, the A^3 line joining $(BA)_{c\beta}$ and $(BA)_{\beta c}$ in Fig. 10(c) grows shorter and eventually these points merge at a tricritical point when the energy point reaches the solid curve in Fig. 10(a). The system phase diagram in which the tricritical point actually occurs is topologically similar (as one might expect) to that shown in Fig. 5(b) [where, it should be noted, the prism has a different orientation from Fig. 10(c)] rather than Fig. 5(f). That is, one does *not* see three lines of critical points coming together at the tricritical point. The reason for this has been discussed elsewhere.[15] It turns out that a diagram of the form in Fig. 5(f) can only be expected in the presence of appropriate symmetries, and the merging of two critical end points, of the sort we have just discussed, is the more common "label" for a tricritical point in the absence of any symmetry.

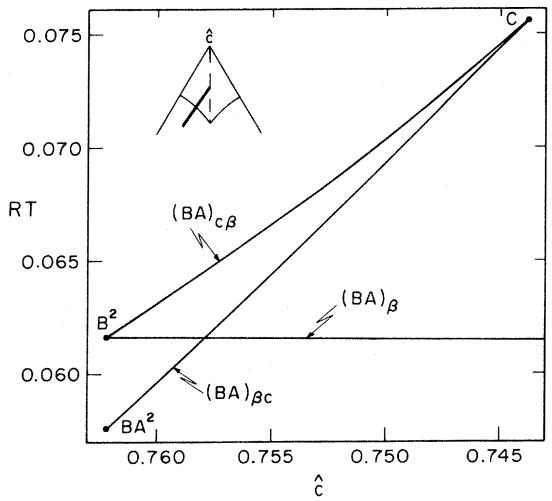

FIG. 11. Critical end points and tricritical point for a section in the energy space ($\hat{b} = 0.118\,924$) indicated by the heavy line in the insert. The drawing is to scale.

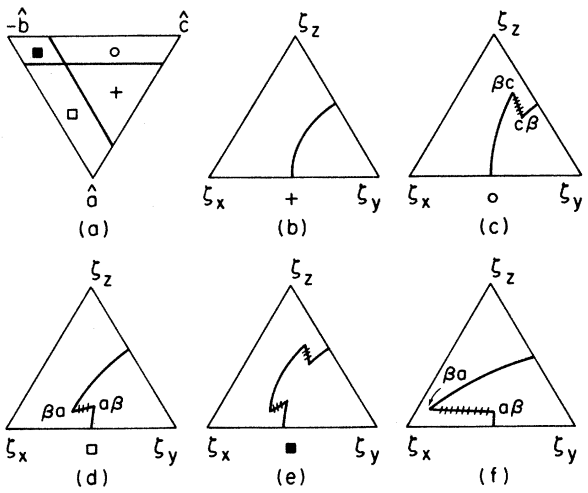

FIG. 12. System phase diagrams (schematic) in one of the Q energy triangles.

The $(BA)_\beta$ point in Fig. 10(c) is not affected by the merging of the other critical end points as the energy point in Fig. 10(a) moves through the line $C_{c\beta}$ into the P_β region of Fig. 3, and hence belongs to the same manifold of β-type critical end points described previously.

In considering the distinction between the two types of three-phase region indicated in Fig. 10(c), which we shall call $(A^3)_1$ and $(A^3)_{c\beta}$, the former extending to zero temperature, it is useful to show "typical" examples in the composition space at a fixed temperature, as in Figs. 9(b) and 9(c). As the energy point approaches the symmetry line $\hat{a} = \hat{b}$ in Fig. 10(a), the phases in Figs. 9(b) and 9(c) approach those numbered in a corresponding way in Fig. 9(a). The critical end points β, $c\beta$, and βc in these diagrams correspond to phases one and three, two and four, three and four, respectively, coalescing in the presence of the remaining phase.

Some further insight on the locations of the different BA manifolds in the energy space is provided by Fig. 11 which shows a section $\hat{b} = 0.118\,9238$ of the energy space, using T as one coordinate, whose projection on the principal energy triangle is the solid heavy line in the insert.

D. Other energy triangles

1. Triangle $\hat{a}, -\hat{b}, \hat{c}$

As the energy point marked + in Fig. 5(a) moves leftward, the temperature of the critical point in the binary system x,z and that of the corresponding critical end point in Fig. 5(b) decrease and reach zero when + arrives at the $\hat{a},\hat{c}$ edge of the principal energy triangle. In the adjacent Q_β region, Fig. 4, the x,z binary system does not phase separate, and the system phase diagrams show only a single coexistence surface extending between the $\zeta_x\zeta_y$ and $\zeta_y\zeta_z$ sides of the activity prism and surmounted by an unbroken line of critical points connecting those in the binary pairs, as shown in Fig. 12(b).

Similarly one can think of the system diagram in the $Q_{c\beta}$ region as obtained from Fig. 10(c) by moving the open circle in Fig. 10(a) to the left across the boundary of the triangle with the consequence that the coexistence surface extending from the $\zeta_x\zeta_z$ side of Fig. 10(c) disappears and with it the associated triple line and $(BA)_\beta$ point. The resulting phase diagram is shown in projection in Fig. 12(c). Note that the three-phase region does not extend to zero temperature. [System phase diagrams in the $Q_{a\beta}$ region in Fig. 4, as illustrated in Fig. 12(d), are similar to those in the $Q_{c\beta}$ region if ζ_x and ζ_z are interchanged.]

The $(A^3)_{c\beta}$ manifold outside the principal triangle, as well as the five other three-phase manifolds related to it by permutation, have been overlooked in previous studies of the three-component model.[1,10] The corresponding type of three-phase coexistence in the van der Waals model of a binary compressible fluid has been pointed out by Scott and Van Konynenburg.[11]

In the Q_{ac} $(=Q_{ca})$ region the system diagrams, as in Fig. 12(e), represent a "superposition" of the triple lines and corresponding critical end points from the diagrams of the $Q_{c\beta}$ and $Q_{a\beta}$ regions. Note that the corresponding three-phase manifolds, $(A^3)_{c\beta}$ and $(A^3)_{a\beta}$, do not meet in the full five-dimensional field space even though they project on

top of each other in the Q_{ac} region of the energy triangle.

2. Triangle $\hat{a}, -\hat{b}, -\hat{c}$

As the energy point marked by an open square in Fig. 12(a) approaches the $\hat{a}, -\hat{b}$ side of the energy triangle, both the βa and $a\beta$ critical end points in Fig. 12(d) tend toward zero temperature. However, the βa point also approaches closer and closer to the ζ_x edge while the $a\beta$ point becomes very close to the $\zeta_x\zeta_y$ side of the prism, as shown in Fig. 12(f). When the energy point reaches the $\hat{a}, -\hat{b}$ side and $\hat{c}$ goes to zero, so that the x, y binary no longer shows phase separation, the A^3 region with its associated critical end points disappears entirely and there is a single line of critical points extending from the $\zeta_y\zeta_z$ side at finite temperatures to the ζ_x edge of the prism *at zero temperature*. Such a system diagram, shown in Fig. 13(b), is characteristic of the R_x region in Fig. 4.

An analogous phenomenon occurs as the solid square in Fig. 12(a) moves leftwards to the $\hat{a}, -\hat{b}$ edge of the triangle. However, the βc and $c\beta$ critical end points and the triple line connecting them are not directly affected by what happens to the $(A^3)_{a\beta}$ region, and they continue to exist as an interruption in the critical line extending from the $\zeta_y\zeta_z$ side of the prism—which now, however, as in Fig. 13(c), characteristic of the $R_{c\beta}$ region in Fig. 4, extends to zero temperature in the ζ_x corner.

3. Triangle $-\hat{a}, -\hat{b}, -\hat{c}$

If the energy point shown as a solid circle in Fig. 13(a) is moved to the left, the $(A^3)_{c\beta}$ region

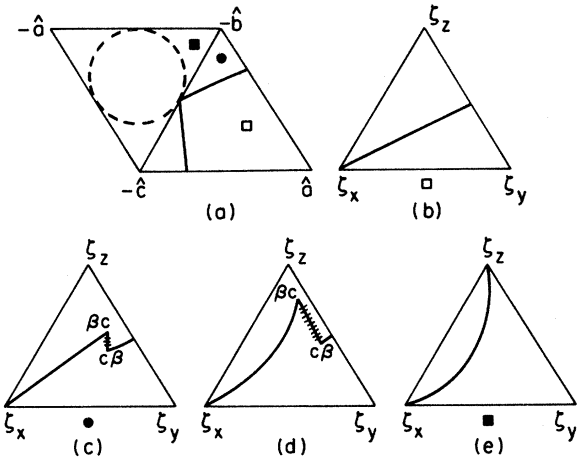

FIG. 13. System phase diagrams (schematic) in the S and one of the R energy triangles.

and its associated critical end points undergo a fate similar to that of the $(A^3)_{a\beta}$ region described previously. This is illustrated in Fig. 13(d). When the energy point reaches the $-\hat{b}, -\hat{c}$ edge of the triangle, there remains only a single critical line extending from the ζ_x to the ζ_z edges of the prism and going to zero temperature at either end, a diagram which characterizes the S_{xz} region in Fig. 4. If the solid square in Fig. 13 is moved to the left, the maximum critical temperature along the line of critical points decreases and reaches zero when the energy point meets the dashed circle. In the region S_0 the potential $\overline{G}$ in Eq. (2.3) is always convex, so there is no phase separation at all.

E. Qualitative description of different manifolds

1. Introduction

We have seen that various features of the global phase diagram, such as points of three-phase coexistence, tricritical points, etc., lie on continuous "surfaces" or manifolds of appropriate dimensionality in the five-dimensional field space spanned by $\overline{a}$, $\overline{b}$, $\overline{c}$, ν_1, and ν_2. By specifying how these manifolds are connected together, one can describe important topological properties[12] of the global phase diagram. Although such properties may appear somewhat abstract, especially as we are describing an object (the phase diagram) in a five-dimensional space, they are of interest because it is precisely the qualitative features of this type which one expects to be the same in the three-component model and in real systems (see Sec. V).

Each point in the field space can be classified as a particular "type" depending on the state of the system which is realized for this choice of thermodynamic variables. For example, if a "critical" phase coexists with another distinct phase, the corresponding "type" is BA. Points of a given type lie on one of (possibly) several distinct manifolds in the global phase diagram. Two BA points, for example, lie on the same manifold if it is possible to connect them by a continuous path in the five-dimensional space which consists entirely of points of type BA and no points of any other type. The different manifolds are labeled with subscripts: $(BA)_\alpha$, $(BA)_\beta$, etc. Note that whereas $(BA)_\alpha$ and $(BA)_\beta$ have common boundary points (their closures, in the usual topology, have nonempty intersections), these points are always of a type other than BA, for instance C or BA^2. We shall say that two manifolds belong to the same "class" if one is mapped into the other by one of the permutation symmetries of the global phase diagram. Thus $(BA)_\alpha$, $(BA)_\beta$, and $(BA)_\gamma$ constitute one class.

Distinct manifolds of points of a given type in the

TABLE III. Numerical values for selected entities. The first column gives the dimension d of the manifold indicated in the second column. The energy parameters $\bar{a}$, $\bar{b}$, $\bar{c}$ and the compositions x and y of representative points are listed in the remaining columns. In the case of a compound entity the location of the second phase is given in columns x' and y', while x and y always refer to the critical phase (e.g., C in CA). A third phase, as in $(BA^2)_{\alpha\gamma}$, is listed under the x'' and y'' columns. Note that a variety of other points may be obtained from those listed by using permutation symmetry.

					Location	
d	Manifold	$\bar{c}$	$\bar{b}$	$\bar{a}$	x	y
0	D_c	$\frac{1}{x}$	$\frac{1}{2x}\ \frac{2x+1}{4-8x}$	$\frac{1}{2x}\ \frac{2x+1}{4-8x}$	$(2+\sqrt{40})^{-1}$	$(2+\sqrt{40})^{-1}$
0	$(CA)_\gamma$	2.465	2.959	2.959	0.4057 0.0943 [a]	0.4057 0.0943 [a]
1	C_c	$\frac{8-6\hat{c}}{4-5\hat{c}}$	$\frac{1-\hat{c}}{2\hat{c}}\ \frac{8-6\hat{c}}{4-5\hat{c}}$	$=\bar{b}$	$=\frac{1}{\bar{c}}$	$=\frac{1}{\bar{c}}$
1	$C_{c\beta}$	0.8875×10	0.1735×10	0.1747×10	0.5521×10^{-1}	0.2004
		0.9593×10	0.1668×10	0.1800×10	0.3078×10^{-1}	0.2461
		0.1005×10^{2}	0.1430×10	0.1833×10	0.2039×10^{-1}	0.2730
		0.1029×10^{2}	0.7919	0.1865×10	0.1299×10^{-1}	0.2985
		0.1026×10^{2}	0.4896	0.1873×10	0.1139×10^{-1}	0.3053
		0.1022×10^{2}	0.2732	0.1878×10	0.1051×10^{-1}	0.3092
		0.1015×10^{2}	0.1982×10^{-2}	0.1883×10	0.9628×10^{-2}	0.3135
		0.1003×10^{2}	−0.3447	0.1888×10	0.8731×10^{-2}	0.3182
		0.9537×10	-0.1414×10	0.1900×10	0.6897×10^{-2}	0.3288
		0.8693×10	-0.2858×10	0.1911×10	0.5477×10^{-2}	0.3386
		0.7488×10	-0.4653×10	0.1919×10	0.4424×10^{-2}	0.3471
		0.6403×10	-0.6150×10	0.1925×10	0.3838×10^{-2}	0.3525
		0.4749×10	-0.8315×10	0.1931×10	0.3242×10^{-2}	0.3587
		0.3113×10	-0.1037×10^{2}	0.1935×10	0.2838×10^{-2}	0.3633
		0.1976×10	-0.1176×10^{2}	0.1938×10	0.2621×10^{-2}	0.3660
		0.1102×10	-0.1282×10^{2}	0.1939×10	0.2480×10^{-2}	0.3679
		0.7486	-0.1325×10^{2}	0.1940×10	0.2427×10^{-2}	0.3681
		0.9473×10^{-1}	-0.1420×10^{2}	0.1941×10	0.2337×10^{-2}	0.3699
		−0.8558	-0.1515×10^{2}	0.1942×10	0.2219×10^{-2}	0.3715
		-0.2878×10	-0.1752×10^{2}	0.1952×10	0.2009×10^{-2}	0.3747
		-0.5488×10	-0.2053×10^{2}	0.1948×10	0.1797×10^{-2}	0.3782
		-0.8957×10	-0.2447×10^{2}	0.1951×10	0.1582×10^{-2}	0.3820
		-0.1375×10^{2}	-0.2982×10^{2}	0.1955×10	0.1365×10^{-2}	0.3863
		-0.2074×10^{2}	-0.3751×10^{2}	0.1958×10	0.1144×10^{-2}	0.3912
		-0.5102×10^{2}	-0.6998×10^{2}	0.1968×10	0.6915×10^{-3}	0.4041
		-0.1539×10^{3}	-0.1769×10^{3}	0.1978×10	0.3105×10^{-3}	0.4214
		-0.3023×10^{4}	-0.3068×10^{4}	0.1994×10	0.2137×10^{-4}	0.4597
1	$(B^2)_c$	8.325	1.699	$=\bar{b}$	0.1215	0.1188 [b]
		9.100	1.768	$=\bar{b}$	0.2794	0.2849×10^{-1}
		1.590×10	1.981	$=\bar{b}$	0.4821	0.2264×10^{-3}
		2.309×10	1.999	$=\bar{b}$	0.4986	0.4986×10^{-3}

TABLE III *(Continued)*

d	Manifold	$\bar{c}$	$\bar{b}$	$\bar{a}$	Location x	y	x'	y'	x''	y''
1	$(BA^2)_{\alpha\gamma}$	2.883	2.721	2.721	0.2500	0.2500	0.7027	0.1379	0.1379	0.7027
		2.892	2.626	2.814	0.2800	0.2255	0.6472	0.1547	0.1219	0.7470
		2.903	2.586	2.852	0.2993	0.2142	0.6112	0.1639	0.1140	0.7670
		2.917	2.546	2.889	0.3189	0.2053	0.5741	0.1718	0.1074	0.7826
		2.930	2.516	2.916	0.3372	0.1990	0.5393	0.1779	0.1026	0.7937
		2.940	2.496	2.934	0.3532	0.1947	0.5085	0.1822	0.9923×10^{-1}	0.8010
		2.945	2.487	2.941	0.3617	0.1929	0.4921	0.1840	0.9781×10^{-1}	0.8041
1	$(BA^2)_c$	9.148	1.776	$=\bar{b}$	0.1093	$=x$	0.3824	0.1303	$=y'$	$=x'$
		1.186×10	1.980	$=\bar{b}$	0.8435×10^{-1}	$=x$	0.6732	0.3851×10^{-3}	$=y'$	$=x'$
		1.859×10	2.324	$=\bar{b}$	0.5379×10^{-1}	$=x$	0.8130	0.2217×10^{-3}	$=y'$	$=x'$
		3.138×10	2.738	$=\bar{b}$	0.3186×10^{-1}	$=x$	0.9004	0.481×10^{-12}	$=y'$	$=x'$
2	$(BA)_{c\beta}$	1.156×10	1.818	1.903	0.3506×10^{-2}	0.4152	0.2035	0.2608×10^{-1}		
		1.591×10	-1.620×10^{-1}	1.987	0.1116×10^{-3}	0.4863	0.1206	0.2360×10^{-1}		
		1.125×10	-5.355	1.983	0.1484×10^{-3}	0.4799	0.5359×10^{-1}	0.7357×10^{-1}		
		1.558	-1.518×10	1.974	0.2607×10^{-3}	0.4651	0.1992×10^{-1}	0.1599		
2	$(BA)_{\beta c}$	1.203×10	1.891	1.980	0.6708×10^{-1}	0.1013	0.3068×10^{-3}	0.6309		
		1.825×10	-6.497×10^{-2}	2.267	0.2730×10^{-1}	0.8954×10^{-1}	0.8821×10^{-7}	0.7893		
		1.167×10	-6.061	2.115	0.1413×10^{-1}	0.1565	0.1066×10^{-5}	0.7085		
3	$(A^3)_{c\beta}$	1.269×10	1.980	1.981	0.2408	0.1346	0.1311×10^{-1}	0.2434	0.2657×10^{-3}	0.6103

[a] The phase labeled by a is the noncritical phase of $(CA)_\gamma$.
[b] The other critical coexisting phase of $(B^2)_c$ is given by $x'=y$, $y'=x$.

TABLE IV. Manifolds and their boundaries. A representative example from each class of manifolds, with the exception of B and A^2, is listed in the first column followed by its dimensionality d and its symmetry number s, the number of manifolds in the class. The last column gives the manifolds of dimension $d-1$ lying on its boundary. For $d=2$ the manifolds on the boundary are listed in order proceeding continuously along the edge of the manifold. All manifolds at zero temperature are labeled (n) (see text).

Manifold	d	s	Boundary	Manifold	d	s	Boundary
D_c	0	3		$(BA)_\beta$	2	3	$(B^2)_a$, C_a, $(BA^2)_{\alpha\beta}$ $(BA^2)_{\beta\gamma}$, C_c, $(B^2)_c$, (n)
$(CA)_\gamma$	0	3					
C_c	1	3	D_c, $(CA)_\gamma$	$(A^4)_I$	2	1	$(BA^2)_{\alpha\beta}$, $(BA^2)_{\beta\gamma}$, $(BA^2)_{\alpha\gamma}$
$C_{c\beta}$	1	6	D_c, (n)	$(A^4)_c$	2	3	$(B^2)_c$, $(BA^2)_c$
$(BA^2)_{\alpha\gamma}=(BA^2)_{\gamma\alpha}$	1	3	$(CA)_\alpha$, $(CA)_\gamma$	$(A^3)_{c\beta}$	3	6	$(BA)_{c\beta}$, $(BA)_{\beta c}$ $(A^4)_c$, (n)
$(B^2)_c$	1	3	D_c, (n)				
$(BA^2)_c$	1	3	D_c, (n)	$(A^3)_I$	3	1	$(BA)_\alpha$, $(BA)_\beta$, $(BA)_\gamma$ $(A^4)_a$, $(A^4)_b$, $(A^4)_c$
$(BA)_{c\beta}$	2	6	$(B^2)_c$, $C_{c\beta}$, (n)				
$(BA)_{\beta c}$	2	6	$(BA^2)_c$, $C_{c\beta}$, (n)				$(A^4)_I$, (n)

global phase diagram we are discussing may well be (and indeed probably are) parts of a single manifold in a higher-dimensional field space obtained by adding additional parameters to the model, e.g., terms such as x^2y, etc., in Eq. (2.3). This does not reduce the value of distinguishing these manifolds in the global phase diagram of the three-component model, though it suggests that one should exercise caution before drawing far-reaching conclusions about real systems from this model.

Each d-dimensional manifold is bounded by manifolds of dimension $d-1$, and these in turn by manifolds of dimension $d-2$, etc. These lower-dimensional manifolds may represent points of a distinct type (e.g., BA^2 manifolds on the boundary of A^4), or points of the same type which lie on the boundary of the phase diagram. Table IV lists one representative from each class of manifolds, aside from A^2 and B, and indicates the manifolds of dimension one less which lie on its boundaries. The same information for other manifolds in a given class can be obtained by applying permutations to the subscripts a, b, c, and simultaneously α, β, γ. Certain boundaries occur at zero temperature, that is to say as $|\vec{a}|+|\vec{b}|+|\vec{c}|$ tends to infinity. All such cases are indicated by (n) in Table IV. One could introduce a more specific labeling based on the discussion in Secs. III C and III D above, but this did not seem to us to be worth the effort.

2. *Zero- and one-dimensional manifolds*

Two classes of zero-dimensional manifolds occur in the global phase diagram: the three D and three CA points shown in Fig. 3. The one-dimensional manifolds include nine C lines belonging to two classes: three lines lying in symmetrical sections Σ_{ab}, etc., which project entirely within the principal energy triangle, Fig. 3, and six which lie outside the symmetrical sections and appear as curved solid lines in Fig. 4. Each of the latter extends from a D point to a point at zero temperature and has a projection which falls in three different energy triangles. These C manifolds are smooth curves, and the kinks which occur at boundaries of the triangles in Fig. 4 are the effect of the projection.

The other classes of one-dimensional manifolds are three BA^2 lines shown as dashed curves in Fig. 3(b), each extending between two CA points, and three B^2 lines and three BA^2 lines which bound the $(A^4)_{II}$ regions, as shown in Fig. 8, and project on top of each other as the straight dashed lines in the principal triangle in Figs. 3(a) and 4.

3. *Two-dimensional manifolds*

There are five classes of two-dimensional manifolds: the $(A_4)_I$ region, the $(A_4)_{II}$ regions, and those represented by $(BA)_\alpha$, $(BA)_{\beta c}$, and $(BA)_{c\beta}$. Each of these manifolds is topologically equivalent to a disk (rather than, for example, a Moebius strip). The $(A^4)_I$ manifold is bounded by three lines, the dashed curves in Fig. 3(b), and each $(A^4)_{II}$ manifold by a BA^2 line and a B^2 line, as shown in Fig. 8.

The $(BA)_{c\beta}$ and $(BA)_{\beta c}$ manifold project on top of each other (with the former at a higher temperature than the latter for a given $\hat{a}$, $\hat{b}$, $\hat{c}$) on the regions denoted by $P_{c\beta}$, $Q_{c\beta}$, Q_{ac}, and $R_{c\beta}$ in Figs. 3 and 4. Both extend to zero temperature (but to different points in the activity triangle) at the $-\hat{b}$, $-\hat{c}$ and $-\hat{b}$, $\hat{c}$ edges of the corresponding energy triangle, and they both terminate on the manifold $C_{c\beta}$. Inside the principal energy triangle, $(BA)_{c\beta}$ terminates at $(B^2)_c$, and $(BA)_{\beta c}$ at $(BA^2)_c$.

The $(BA)_\beta$ manifold projects on the $P_{a\beta}$, P_β, and

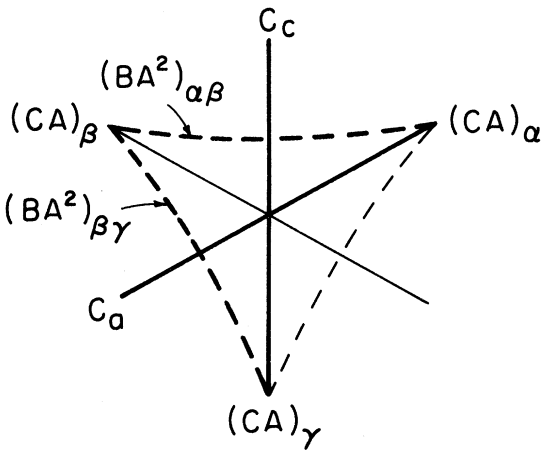

FIG. 14. Heavy solid and dashed lines indicate the boundaries of the $(BA)_\beta$ manifold near the center of the principal energy triangle.

$P_{c\beta}$ regions of the principal energy triangle, Fig. 3, and goes to zero temperature along the $\hat{a},\hat{c}$ edge. It terminates on the $(B^2)_a$ and $(B^2)_c$ manifolds near the $\hat{a}$ and $\hat{c}$ corners, as well as the C_a and C_c manifolds. However, near the center of the principal energy triangle its behavior in projection is rather complicated. The actual boundary is shown by the heavy lines, solid and dashed, in Fig. 14, which shows the same projection as Fig. 3(b), and consists of the lines and points C_a, $(CA)_\alpha$, $(BA^2)_{\alpha\beta}$, $(CA)_\beta$, $(BA^2)_{\beta\gamma}$, $(CA)_\gamma$, C_c. The manifold projects once on the regions [Fig. 3(b)] $P_{\alpha\beta}$ and $P_{\gamma\beta}$, and *twice* on the regions $P_{\beta\alpha}$ and $P_{\beta\gamma}$.

4. *Three-dimensional manifolds*

The only three-dimensional manifolds in the global phase diagram are of type A^3 and occur in two classes: the $(A^3)_{\mathrm{I}}$ manifold and the six of which $(A^3)_{c\beta}$ is a representative. The manifold $(A^3)_{c\beta}$ is, we believe, topologically equivalent to a three-ball and is bounded by the two-dimensional surfaces $(BA)_{c\beta}$, $(BA)_{\beta c}$, $(A^4)_c$, and one at zero temperature. It projects on the same region in the energy triangles as $(BA)_{c\beta}$ and $(BA)_{\beta c}$, and reaches zero temperature only at the edges of the triangles where the latter manifolds go to zero temperature (see discussion above).

The manifold $(A^3)_{\mathrm{I}}$ is more complicated. It projects on the entire principal energy triangle and on no other triangle. For a fixed $\hat{a}$, $\hat{b}$, and $\hat{c}$, it extends from $T=0$ up to a temperature where it terminates on a $(BA)_\alpha$, $(BA)_\beta$, or $(BA)_\gamma$ manifold. However, the $(A^4)_{\mathrm{I}}$ and $(A^4)_{\mathrm{II}}$ manifolds also lie on the boundary of $(A^3)_{\mathrm{I}}$ in a manner which must be described with some care. In a three-dimensional section of the field space, each A^4 point is the terminus of four lines of A^3 points. For points on the $(A^4)_c$ manifold, one of these A^3 lines belongs to $(A^3)_{c\beta}$, one to $(A^3)_{c\alpha}$, and *two* to $(A^3)_{\mathrm{I}}$. For points on the $(A^4)_{\mathrm{I}}$ manifold, all four A^3 lines belong to $(A^3)_{\mathrm{I}}$. Thus the A^4 manifolds are not simple boundaries of $(A^3)_{\mathrm{I}}$, and the latter is not topologically equivalent to a ball.

5. *Manifolds A^2 and B*

An examination of the various system phase diagrams and their variation as the corresponding energy point is displaced shows that all A^2 points belong to the same four-dimensional manifold, and all B points to the same three-dimensional manifold. Naturally these manifolds are topologically rather complicated, and we shall not attempt to describe them. It is perhaps worth noting that they, unlike any of the other manifolds discussed above, intersect the boundaries of the phase diagram at places other than zero temperature, namely, in the binary mixtures (e.g., $\zeta_z=0$).

IV. MATHEMATICAL METHODS

A. Elementary entities

The existence of the "elementary" entities B, C, and D (in contrast to "composite" entities A^2, BA, etc.) depends on properties of the $\bar{G}(x,y)$ surface in the immediate vicinity of a single point. It is convenient to consider first the conditions which must be satisfied by a potential $\bar{h}(r)$ depending on a *single* density variable r so than an nth-order critical point ($n=2$, 3, and 4 for B, C, and D, respectively) occurs at $r=r_1$. These are

$$\frac{d^m\bar{h}}{dr^m}=0 \quad \text{for } 2\leq m\leq 2n-1, \tag{4.1}$$

$$\frac{d^{2n}\bar{h}}{dr^{2n}}>0, \tag{4.2}$$

with the derivatives evaluated at $r=r_1$. The condition (4.2), when (4.1) is satisfied, insures that $\bar{h}$ is a convex function in the immediate vicinity of $r=r_1$, and can thus be called a condition of "local stability." There is an additional condition of "global stability," that $\bar{h}$ coincide with its convex hull at $r=r_1$, which must be satisfied if the entity of interest is to be stable rather than metastable.

It will be convenient to suppose that $\bar{G}$ is expressed as a function of two density variables r and s which are linear (or affine) functions of x and y. Such a change of variables is convenient rather than essential, and the existence of a (higher-order) critical point is not dependent on the precise choice of r and s. Let us consider the conditions which $\bar{G}$ must satisfy for an nth-order critical point at (r_1,s_1). Define the field variable

Δ by

$$\Delta = \frac{\partial \bar{G}}{\partial s} = \bar{G}_s \tag{4.3}$$

and let Δ_1 be its value at (r_1, s_1). Also assume that at this point

$$\bar{G}_{ss} = \frac{\partial^2 \bar{G}}{\partial s^2} > 0. \tag{4.4}$$

Then for Δ near Δ_1, s near s_1, and r near r_1, we can introduce the Legendre transformation

$$\bar{h}(r, \Delta) = \bar{G}(r, s) - \Delta s, \tag{4.5}$$

where s, on the right-hand side, is the (unique) function of r and Δ defined by (4.3). Then the condition that $\bar{G}$ have an nth-order critical point at (r_1, s_1) is that (4.1) and (4.2) be satisfied for $\bar{h}(r, \Delta_1)$ regarded as a function of r. In addition, there is a requirement of global stability, that $\bar{G}$ coincide with its convex hull G at the point of interest, which will be discussed in Sec. IV B below.

It is possible to reexpress the conditions (4.1) and (4.2) for $\bar{G}$ in a form which makes less explicit use of a particular choice of coordinate axes. Thus (4.1) for $m = 2$, with (4.4), turns out to be equivalent to the assertion that the determinant of the Hessian matrix

$$\begin{pmatrix} \bar{G}_{rr} & \bar{G}_{rs} \\ \bar{G}_{sr} & \bar{G}_{ss} \end{pmatrix} \tag{4.6}$$

vanishes, or that this matrix has one zero and one positive eigenvalue. Given this last condition, it is always possible to choose coordinates r and s such that (4.4) is satisfied; but note that for a specific choice of axes, a (higher-order) critical point may occur where $\bar{G}_{ss} = 0$, in which case the discussion in terms of (4.5) and (4.1) is inapplicable. In principle, there can also be higher-order critical points for which both eigenvalues of the Hessian matrix are zero[12] and which are not encompassed in the classification scheme embodied in (4.1) and (4.2). These do not, however, occur, so far as we can tell, in the three-component model under discussion.

In the case of ordinary critical points B, $n = 2$, it is possible to write the two equations (4.1) in the symmetrical form (see Ref. 8):

$$\frac{x}{1 - x(\bar{b} + \bar{c} - \bar{a})} + \frac{y}{1 - y(\bar{a} + \bar{c} - \bar{b})} + \frac{z}{1 - z(\bar{a} + \bar{b} - \bar{c})} = 0, \tag{4.7}$$

$$\frac{x}{[1 - x(\bar{b} + \bar{c} - \bar{a})]^3} + \frac{y}{[1 - y(\bar{a} + \bar{c} - \bar{b})]^3} + \frac{z}{[1 - z(\bar{a} + \bar{b} - \bar{c})]^3} = 0. \tag{4.8}$$

These equations were solved numerically for a fixed choice of $\hat{a}$, $\hat{b}$, and $\hat{c}$ [see (2.4)] by regarding (4.7) as a quadratic equation in the temperature T and substituting the roots of this equation in (4.8). The resulting equation was then solved numerically and the critical points thereby obtained were checked for global stability. Although global stability insures local stability, it was convenient to first check the latter by means of

$$-2\bar{c} + 1/x + 1/y \geq 0, \tag{4.9}$$

which insures that the eigenvalues of the Hessian (4.6) are non-negative. Equations (4.7)–(4.9) are not applicable to certain critical points occurring in the symmetrical sections Σ_{ab}, etc., which are discussed separately below in Sec. IV D.

Tricritical points C, $n = 3$, were investigated with the help of (4.5), (4.1), and (4.2) with the following choice of coordinates:

$$r = x + y = 1 - z, \tag{4.10}$$

$$s = x - y = r\lambda, \tag{4.11}$$

where r lies between 0 and 1, and the parameter λ, equal to s/r, between -1 and $+1$. In terms of these variables $\bar{G}$ has the form

$$\bar{G} = r \ln(\tfrac{1}{2}r) + (1 - r)\ln(1 - r) + \tfrac{1}{4}(\bar{c} - 2\bar{a} - 2\bar{b})r^2 + \tfrac{1}{2}r[(1 + \lambda)\ln(1 + \lambda) + (1 - \lambda)\ln(1 - \lambda) - \tfrac{1}{2}\bar{c}r\lambda^2 + (\bar{a} - \bar{b})r\lambda]. \tag{4.12}$$

At a fixed r, $\bar{G}$ as a function of λ has a form familiar from the mean-field theory of an Ising ferromagnet or the regular solution theory of a binary mixture. One easily shows that a necessary (but not sufficient) condition for global stability with $\bar{c} > 0$ is that

$$\lambda[\ln(1 + \lambda) - \ln(1 - \lambda) - \bar{c}r\lambda] \geq 0, \tag{4.13}$$

as otherwise λ lies in a metastable region. This condition is trivially satisfied for $\bar{c} < 0$ and, except when $\lambda = 0$, insures condition (4.4). As shown in the Appendix, one can obtain a parametric solution to the four equations in (4.1) at the cost of numerically solving a single equation in one unknown. Both (4.2) and (4.13) were applied as checks for stability, and then the tricritical points so obtained were checked for global stability. Condition (4.4) is violated for tricritical points in the symmetrical section Σ_{ab} (though not for the corresponding points in Σ_{ac} and Σ_{bc}), but these can be more easily obtained, in any case, by an alternative calculation (Sec. IV D).

B. Global stability

We used the technique of Ref. 8, with minor modifications, in order to check global stability. The

basic idea is as follows. To check whether a point (x_1, y_1) is stable in a global sense one finds all other points in the triangle (2.6) which have the same chemical potentials

$$\nu_1 = \frac{\partial \overline{G}}{\partial x}, \quad \nu_2 = \frac{\partial \overline{G}}{\partial y} \tag{4.14}$$

as the point in question. At each of these points ν_z is evaluated using (2.9). The point(s) having the minimum value of ν_z is globally stable; the rest are unstable or metastable.

One can very well use alternative coordinates in place of x and y and other choices for the chemical potential. As one of the chemical potentials we used [see (4.3) and (4.10)–(4.12)]

$$\Delta = \tfrac{1}{2} \ln[(1+\lambda)/(1-\lambda)] + \tfrac{1}{2}(\overline{a} - \overline{b})r - \tfrac{1}{2}\overline{c}r\lambda. \tag{4.15}$$

For a fixed choice of Δ, determined by its value at the point (x_1, y_1), (4.15) may be used to generate a curve of r as a function of λ, for $-1 \leq \lambda \leq 1$. There is no loss of generality (and in practice a faster numerical program when $\overline{c}$ is positive) if the parameter λ is restricted to values satisfying (4.13). The remaining chemical potential is easily evaluated as a function of r and thus of λ, and the equation setting this equal to its value at the point (x_1, y_1) is then solved numerically as a function of λ.

C. Compound entities

The "compound" entities such as A^3, BA, etc., depend on the properties of $\overline{G}(x, y)$ in the vicinity of two or more points in the triangle (2.6). The equations for the coexistence of two phases at (x_1, y_1) and (x_2, y_2) are as follows,[1] with $z_j = 1 - x_j - y_j$:

$$(x_1 + x_2) \ln\left(\frac{x_1}{x_2}\right) + (y_1 + y_2) \ln\left(\frac{y_1}{y_2}\right) + (z_1 + z_2) \ln\left(\frac{z_1}{z_2}\right) = 0, \tag{4.16}$$

$$\ln\left(\frac{x_1}{x_2}\right) - \ln\left(\frac{z_1}{z_2}\right) = \overline{b}(x_1 - x_2 - z_1 + z_2) + (\overline{a} - \overline{c})(y_1 - y_2), \tag{4.17}$$

$$\ln\left(\frac{y_1}{y_2}\right) - \ln\left(\frac{z_1}{z_2}\right) = \overline{a}(y_1 - y_2 - z_1 + z_2) + (\overline{b} - \overline{c})(x_1 - x_2). \tag{4.18}$$

They express the fact that ν_x, ν_y (or ν_1, ν_2) and ν_z, Eq. (2.9), must be the same in both phases. For coexistence of three phases one has six equations: the three above, plus three obtained by replacing the subscript 2 everywhere by 3. If one of the phases is a critical point, the equations of criticality, (4.7) and (4.8), must be satisfied at this point. Consequently BA^2 (to take an example) is determined, in general, by eight equations. When certain symmetries are present not all the equations need be independent (see Sec. IV D below).

Once a solution to the equations for a compound entity has been found, it can be checked for global stability. The procedure is identical to that employed for elementary entities, Sec. IV B above. In addition, it is possible to use the global stability check directly for locating compound entities. Suppose, for example, that the equations for a critical point B are solved as a function of temperature at fixed $\hat{a}$, $\hat{b}$, $\hat{c}$, and it is found that the critical points are globally stable above a certain temperature and metastable beneath this temperature. At the lowest temperature where global sta-

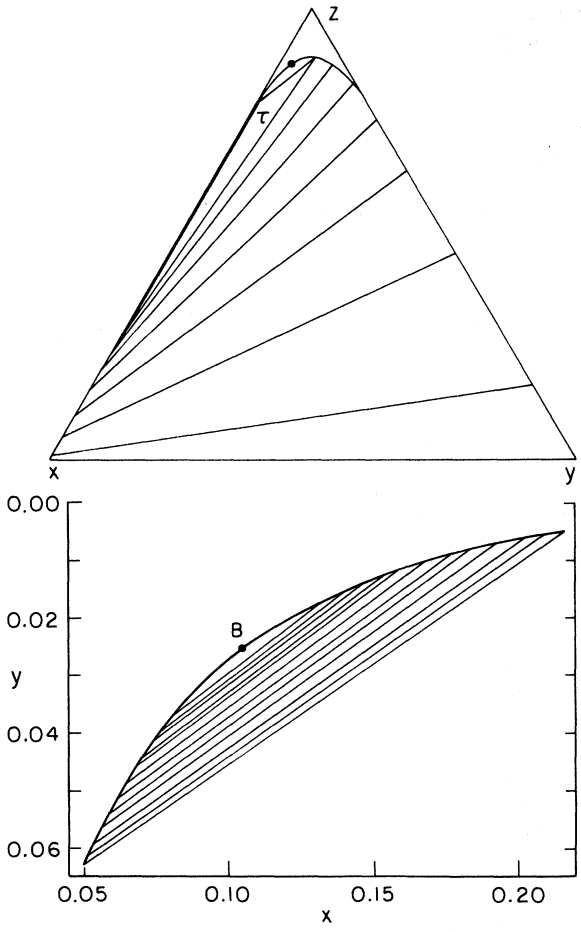

FIG. 15. Phase diagram to scale for the system $\hat{c} = 0.841\,297\,49$, $\hat{b} = 0.109\,033\,59$, $\hat{a} = -0.049\,668\,92$ at $RT = 0.050\,999\,96$. (a) shows a three-phase region at $x_1 = 0.215\,886\,89$, $y_1 = 0.004\,8319$, $x_2 = 0.049\,366\,85$, $y_2 = 0.063\,1138$; $x_3 = 0.722\,1441$, $y_3 = 0.7402 \times 10^{-6}$; and two sets of tie lines. The left-most two-phase region is indistinguishable from the xz side of the composition triangle. (b) An enlargement (in rectangular coordinates) of the binodal in (a) with a critical point. The lowest tie line opposite the critical point in (b) is one leg of the three-phase triangle in (a).

bility is satisfied one has a critical end point BA (or possibly BA^2), and the stability check itself yields the location of the phase A with which B coexists. This procedure is quite effective in locating a particular example of a compound entity, but rather inefficient for exploring a manifold of such entities.

There are special cases (in particular, when symmetries are present) when the equations for a given entity can be solved analytically, in whole or in part. However, this is not possible in general and the equations must be solved numerically. We have found the use of perturbation theory fairly effective in this connection. Thus by linearizing the appropriate equations about a known example of the entity in question, one can calculate approximately the location of the coexisting phases when a parameter (typically T, $\bar{a}$, $\bar{b}$, or $\bar{c}$) is altered by a small amount, and the approximation can be improved by iteration.

In practice we have used a computer routine which evaluates partial derivatives numerically and thus does not require an explicit linearization of the equations. It has been used to locate the manifold $(BA^2)_{\alpha\beta}$ and several points in $(A^4)_{\mathrm{I}}$, $(BA)_{\beta c}$, $(BA)_{c\beta}$, $(BA)_{\alpha}$, $(A^3)_{\mathrm{I}}$, and $(A^3)_{c\beta}$. The diagram in Fig. 11 was constructed in this manner. A perturbation scheme may also be used to generate particular sections of the global diagram as, for example, that shown in Fig. 15, in which both the A^3 triangle and several A^2 tie lines were obtained by perturbation. Such perturbation schemes are easy to write and quite efficient. The data collected in Table III may be used to provide starting points for perturbation calculations.

D. Symmetrical sections

The equations for various entities simplify when they lie in the symmetrical section Σ_{ab}, and some progress can be made towards analytic solutions. In what follows we shall always assume that

$$\bar{a}=\bar{b}. \tag{4.19}$$

Analogous results can be obtained for Σ_{ac} and Σ_{bc} by use of permutations.

In particular, for a "horizontal" tie line, Fig. 16(a), with

$$y_2=x_1, \quad x_2=y_1, \tag{4.20}$$

Eq. (4.16) is satisfied and (4.17) and (4.18) are equivalent to

$$\ln(x_1/y_1)=\bar{c}(x_1-y_1). \tag{4.21}$$

Equation (4.21) for fixed $\bar{c}$ defines a "binodal" curve in the composition triangle, Fig. 16(b); we use quotation marks because the coexisting phases may not be globally stable. A convenient parametric representation of the solution of (4.21) for fixed $\bar{c}$ can be written as

$$y_1=(1/\bar{c})[(\ln q)/(q-1)], \quad x_1=q\,y_1, \tag{4.22}$$

for $0<q<\infty$.

A critical point occurs at $q=1$ or

$$x_1=y_1=1/\bar{c}. \tag{4.23}$$

This "symmetrical" critical point (and its analogs in Σ_{ac} and Σ_{bc}) is not given by Eqs. (4.7) and (4.8), and the condition (4.9) must be modified to read

$$1\geq(\bar{a}+\bar{b}-\bar{c})(1-2/\bar{c}). \tag{4.24}$$

A symmetrical tricritical point C rather than critical point occurs at (4.23) provided

$$\bar{a}=\bar{c}(\bar{c}+2)/8(\bar{c}-2), \tag{4.25}$$

and the fourth-order point D_c occurs when

$$\bar{c}=2+\sqrt{40} \tag{4.26}$$

is inserted in (4.25).[8] The D point is stable, but global stability of the B and C points depends on the values of $\bar{a}$ and $\bar{c}$.

In type-II four-phase coexistence (see Sec. III C 4 above), with the four phases disposed symmetrically as in Fig. 9(a), all four phases lie on the same binodal (4.21). The additional conditions which insure the coexistence of these phases can be taken as (4.16) and (4.17) with 2 everywhere replaced by 3. [One does not need to consider (4.18) because the difference of (4.17) and (4.18), with 2 replaced by 3, vanishes as a consequence of (4.21), and its analog with 1 replaced by 3, being satisfied for the same $\bar{c}$.] The latter may be regarded as defining the value of $\bar{a}$ $(=\bar{b})$ once a solution to the former has been obtained. In particular, using the parametrization (4.22) for both (x_1, y_1) and (x_3, y_3)—with, of course, different choices of q—one obtains a single transcendental equation which can be solved numerically.

In the limit in which phases one and three of Fig. 9(a) coalesce, and consequently also two and four, to form a B^2 point, the transcendental equa-

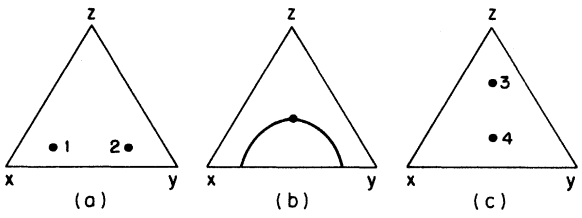

FIG. 16. These drawings illustrate two types of two-phase coexistence, (a) and (c), and binodal, (b), in the symmetrical section Σ_{ab}.

tion simplifies and $\bar{c}$ may be obtained parametrically in terms of q as a solution of

$$[\bar{c}(q-1)-(q+1)\ln q]^2 = \frac{(\ln q)^2(q^2-1-2q\ln q)^3}{q(q-1-\ln q)^3+(q-1-q\ln q)^3}. \quad (4.27)$$

There is no corresponding simplification when phases three and four of Fig. 9(a) coalesce at a BA^2 point, and the values in Table III were obtained by numerical solution of the transcendental equation.

Another simple case of two-phase coexistence in Σ_{ab} is that shown in Fig. 16(c), and given by the formulas[1]

$$x_3=y_3,\quad x_4=y_4,\quad x_3=\tfrac{1}{2}-x_4, \quad (4.28)$$

$$\ln[2x_3/(1-2x_3)]=(\bar{a}-\tfrac{1}{4}\bar{c})(4x_3-1), \quad (4.29)$$

to which one must (as usual) add a stability condition. These equations may be used to find the tricritical end point $(CA)_\gamma$ as follows. The C point is given by $x_4=y_4=\bar{c}^{-1}$ in accordance with (4.23). Setting $x_3=\frac{1}{2}-\bar{c}$ in (4.29) and replacing $\bar{a}$ in this equation by the right-hand side of (4.25), one obtains a transcendental equation in $\bar{c}$ which can be solved to give the result in Table III.

Points of four-phase coexistence of type I in Σ_{ab}, as shown in Fig. 7(d), may be obtained by numerical solution of a single transcendental equation in the following manner. One introduces the parametrization of (4.10) and (4.11):

$$x_1=y_2=\tfrac{1}{2}r(1+\lambda),\quad y_1=x_2=\tfrac{1}{2}r(1-\lambda). \quad (4.30)$$

Also, since (4.28) must be satisfied, we can write

$$x_3=y_3=\tfrac{1}{4}(1+\nu),\quad x_4=y_4=\tfrac{1}{4}(1-\nu) \quad (4.31)$$

with ν another parameter. Next the two equations obtained by replacing 2 by 3, and then 2 by 4, in (4.16) are written down in terms of r, λ, and ν using the above parametrization. The *difference* of these two equations can be solved *explicitly* for λ as a function of r and ν, and the solution inserted in the sum of the two equations, yielding a transcendental equation in r and ν. This is solved numerically for r with ν fixed, and then $\bar{a}$ and $\bar{c}$ are determined by (4.21) and (4.29), as functions of the parameter ν. The case $\nu=0$, in particular, represents the situation in which phases three and four coalesce and one has the BA^2 point at the intersection of $(BA^2)_{\alpha\beta}$ and Σ_{ab}.

In summary, we see that various entities of interest in the symmetrical section Σ_{ab} can be obtained (at least parametrically) with at most the numerical solution of a single transcendental equation. Once a solution in Σ_{ab} is available, it can be used as the starting point of a perturbation calculation for entities outside Σ_{ab}, using the procedures indicated in Sec. IV C.

E. Is the phase diagram complete?

All our numerical studies of specific system phase diagrams and calculations of various other features of the global phase diagram are consistent with the material presented above in Sec. III. There remains the possibility that we have overlooked some regions of A^3 or A^4 (or even A^2) which lie on separate manifolds from those discussed in Sec. III. In the case of A^3 or A^4, one would expect the manifolds to be bounded by BA or BA^2 manifolds, respectively. In turn, BA and BA^2 manifolds cannot terminate in binary mixtures (at finite temperatures), and one might expect to find C and CA manifolds, respectively, on their boundaries.

Our numerical search for C points (Sec. IV A and the Appendix) was nonperturbative and hence capable, in principle, of generating all C points on all manifolds. [Due to the choice of r and s axes, (4.10) and (4.11), our technique does not generate C points in Σ_{ab}, but it does generate the corresponding points in Σ_{ac} and Σ_{bc}.] These points were checked for global stability, and the only CA points discovered were the three in Fig. 3(b). Of course, it is possible that we missed some C points in the numerical search for CA points in the stability check; in these matters one cannot be absolutely certain. Nonetheless, we are reasonably confident that the only manifolds of stable C points are those displayed in Figs. 3 and 4.

It is possible, of course, that a BA manifold would only terminate at zero temperature and never on a C manifold. This is not true of any of the BA manifolds which we have investigated, but there seems to be no argument which rules it out in principle, and no very effective way to search the parameter space to adequately test for such a possibility. We calculated lines of B points in a number of system phase diagrams and tested these for global stability. The results were always consistent with our expectations based on the material presented in Sec. III, but the number of cases investigated was too small to constitute anything approaching a thorough search. Also, the global stability check in such cases is not foolproof, since it requires a numerical search for zeros of functions, and sometimes the functions are of a form which makes this search difficult.

While the possibilities just discussed cannot be ruled out entirely, it is perhaps worth emphasizing that the global phase diagram presented in Sec. III does permit us to assign all the entities we discovered by numerical investigation to ap-

propriate manifolds of the expected[12] codimension (making a suitable allowance for symmetry in some cases), and these manifolds in turn have appropriate entities on their boundaries. This overall consistency is what gives us a fair amount of confidence that our results are, in fact, correct.

V. THREE-COMPONENT MODEL AND REAL SYSTEMS

A. Systems without symmetry breaking

When considering applications of the three-component model phase diagram to real systems, one must exercise judgment in deciding which features of the model should be taken seriously and which are completely artificial. In this connection, it is necessary to distinguish phase transitions involving symmetry breaking (discussed in Sec. V B below) from those in which symmetry breaking plays no essential role, as exemplified by ordinary liquid mixtures.

Consider, for example, a three-component liquid mixture at constant pressure. As there are three adjustable field variables—three thermodynamic degrees of freedom—one might hope that its phase diagram would correspond to some three-dimensional section of the five-dimensional global phase diagram of the three-component model. It is, of course, unrealistic to hope for a strict numerical correspondence between the phase diagrams, but one might hope for a topological correspondence in the sense that the connectivity of n-phase regions, critical manifolds, etc., is given correctly, provided the section is properly chosen. Perhaps other qualitative features (as, for example, two mainfolds meeting in a cusp) would be correctly predicted by the model.

However, one cannot assume that the appropriate section will necessarily correspond to one obtained by fixing $\hat{a}$, $\hat{b}$, and $\hat{c}$ in the model, to what we have called a "system phase diagram" in Sec. III. That is, the appropriate section need not project as a single point in Fig. 4, but might correspond to a "movable point" whose position depends on the temperature and chemical potentials of the real system. A chemical potential for the real system might be some nonlinear combination of the five field variables of the model. Naturally, one hopes that in many applications the chemical potentials of the real ternary system (only two of which are independent if the pressure is fixed) will correspond to those of the model in a first approximation, as this makes it easier to construct an analogy between the two. Perhaps it is worth emphasizing that the sections being considered are smooth surfaces in the field space of the model. Sections with some densities held fixed, or which are smooth surfaces in some space of mixed field and density variables, will in general not resemble the phase diagram of a system with less than five degrees of freedom.

If the pressure of the three-component mixture is varied, or, alternatively, if the pressure is held constant and an additional component with chemical properties similar to one of those already present is added to the mixture, one has a system with four degrees of freedom which might correspond to a four-dimensional section of the global phase diagram of the three-component model. Such a section would project, at the very least, as a line in Fig. 4. This raises the interesting possibility that certain topological features of the global diagram might be tested experimentally.

In this connection it is worth pointing out certain features of the global phase diagram which are decidedly artificial in terms of liquid mixtures. The fact that certain critical lines, etc., extend to zero temperature in the model is clearly artificial. Ordinary mixtures always freeze at sufficiently low temperatures, and the three-component model says nothing at all about the solid phases. Furthermore, the presence of fourth-order critical points D, Fig. 3(a), is artificial, as these points have codimension 6, i.e., should not be observed unless a system has six field variables.[12] They appear in the global phase diagram of the three-component model because of a symmetry. Likewise a one-dimensional B^2 manifold (B^2 has codimension 5) terminating the $(A^4)_{II}$ region is a consequence of symmetry. Hence in a real system with five field variables one cannot expect three C lines and a B^2 line to come together at a D point as in Fig. 3, unless the system has an appropriate symmetry which is absent in ordinary liquid mixtures.

By contrast, all the entities in the "shield" region in Fig. 3(b) have appropriate codimension, and thus such a region might well occur in a phase diagram for a suitable liquid mixture. Of course, one would not expect the threefold symmetry of the diagram in Fig. 3(b); for a real system such a projection would be distorted, but (we expect) connected together in the same fashion with three tricritical lines, a four-phase region, etc.

It is, of course, not impossible that a completely different behavior will be observed in real mixtures in the vicinity of what corresponds to the "shield" region in the model. For example, one could imagine the three tricritical lines simply converging at a single higher-order critical point, as shown in Fig. 17. There is some evidence[16] that this is the case for the lattice gas, Eq. (2.16) or (2.23), in two dimensions, provided the sta-

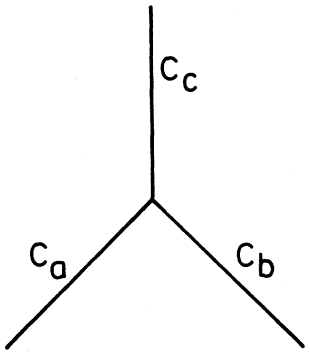

FIG. 17. Possible modification of the "shield" region, Fig. 3(b), with a special tricritical point where the three C manifolds come together.

tistics are treated properly and not in a mean-field approximation. An experimental search for the "shield" region in real mixtures might prove interesting.

B. Systems with symmetry breaking

In many applications of the three-component model, one is concerned with phase transitions in which the symmetry group of the system changes as the temperature or pressure, etc., is varied. Antiferromagnetism and order-disorder transitions in alloys are two examples. In such situations it is usually one of the symmetrical sections of the global phase diagram which is of interest, although if symmetry-breaking thermodynamic variables (such as a magnetic field in the case of ferromagnets) are present, one may also be concerned with what happens outside the symmetrical section.

Let us consider the section Σ_{ab} in which

$$\bar{a} = \bar{b}, \quad \zeta_x = \zeta_y. \tag{5.1}$$

This contains a number of interesting features in the principal energy triangle, as first pointed out by Meijering,[2] and nothing very interesting in the other energy triangles. The presence of D and a one-dimensional B^2 manifold, see Fig. 8, is not an artificial feature of the model in this case, in contrast to the situation with liquid mixtures.

We might expect the phase diagram for a real system with one thermodynamic degree of freedom (say the temperature) to correspond to a one-dimensional section of Σ_{ab}. However, it need not correspond to constant $\hat{c}$, i.e., the line need not appear as a vertical, or even as a straight, projection in Fig. 8. Similar remarks apply in the case of a system with additional thermodynamic variables (assuming they do not, of themselves, break the symmetry). One should expect qualitative rather than quantitative agreement.

Features of particular interest in the Σ_{ab} section are the fourth-order point D and the tricritical end point CA, neither of which has yet been observed experimentally in real systems. There is some indication[17] that B^2 and BA^2 points may occur in the antiferromagnet $FeBr_2$, and it may be worthwhile searching for a system in which an additional parameter can be varied so as to make such a pair of points coalesce in a D point. The CA point occurs at one cusp of the shield region in Fig. 3(b). Since there is some question as to whether the shield will be observed in real liquid mixtures (see Sec. V A above), it is also of some interest to know whether such a CA will actually occur in a system with symmetry breaking.

APPENDIX: EQUATION FOR TRICRITICAL POINTS

With r, s, and λ defined in (4.10) and (4.11), let

$$h(r, s; \Delta) = \bar{G}(r, s) - \Delta s = g_1(r) + k(r, \lambda), \tag{A1}$$

where

$$g_1(r) = [\tfrac{1}{2}(\bar{a} + \bar{b}) - \ln 2]r + r \ln r + (1 - r)\ln(1 - r) - \eta r^2, \tag{A2}$$

$$k(r, \lambda) = \tfrac{1}{2} r \ln(1 - \lambda^2) + \tfrac{1}{2} r\lambda[\ln(1 + \lambda) - \ln(1 - \lambda)] - \tfrac{1}{4}\bar{c}\, r^2\lambda^2 - \tfrac{1}{2}(\bar{a} - \bar{b})\, r(1 - r)\lambda - \Delta r\lambda, \tag{A3}$$

$$\eta = \tfrac{1}{2}(\bar{a} + \bar{b} - \tfrac{1}{2}\bar{c}\,). \tag{A4}$$

We shall assume throughout the following discussing that Δ is fixed. The function $\bar{h}$, (4.5), is the minimum of h with respect to s or, equivalently, with respect to λ, at a fixed value of r. Thus the derivatives in (4.1) are equal to the corresponding derivatives of h along the curve

$$\left(\frac{\partial k}{\partial \lambda}\right)_r = k_\lambda = 0, \tag{A5}$$

where subscripts r and λ on k denote the corresponding partial derivatives.

If d/dr denotes the derivative with respect to r along the curve (A5), we may write

$$\frac{d^m \bar{h}}{dr^m} = \frac{d^m h}{dr^m} = \frac{d^m g_1}{dr^m} + \frac{d^m k}{dr^m}, \tag{A6}$$

where the derivatives of g_1 are easily written down, whereas those of k have the form

$$\frac{dk}{dr} = k_r + k_\lambda \frac{d\lambda}{dr} = k_r, \tag{A7}$$

$$\frac{d^2k}{dr^2} = k_{rr} + k_{r\lambda}\frac{d\lambda}{dr}, \tag{A8}$$

etc. The derivatives $d\lambda/dr$, $d^2\lambda/dr^2$, etc., may be eliminated from $d^m k/dr^m$ by using the equations ($n = 1$, 2, etc.)

$$\frac{d^n k_\lambda}{dr^n} = 0 \tag{A9}$$

obtained by differentiating (A5).

If we introduce the variables

$$\bar{\alpha} = \bar{c}r, \quad \bar{\zeta} = \tfrac{1}{2}(\bar{a} - \bar{b})r, \tag{A10}$$

it turns out that

$$\frac{d^m k}{dr^m} = \frac{f_m}{r^{m-1}}, \tag{A11}$$

where the f_m depend on λ, $\bar{\alpha}$ and $\bar{\zeta}$, but have no explicit r dependence. Using this result, one can rewrite (4.1) [which is equivalent to setting (A6) equal to zero] for $m = 3$, 4, and 5 in the form

$$\begin{aligned} R^2 &= 1 - f_3 = w, \\ R^3 &= -(1 + \tfrac{1}{2}f_4) = \tfrac{3}{2}tX - u, \\ R^4 &= 1 - \tfrac{1}{6}f_5 = v - \tfrac{10}{3}(u - w)X + \tfrac{5}{2}(2t - w + 1)X^2, \end{aligned} \tag{A12}$$

where

$$\begin{aligned} R &= r/(1 - r), \\ w &= 1 + 3t_1 + t_2, \\ t &= 2t_1 + t_2, \\ u &= 1 + 6t_1 + 4t_2 + \tfrac{1}{2}t_3, \\ v &= 1 + 10t_1 + 10t_2 + \tfrac{5}{2}t_3 + \tfrac{1}{6}t_4, \\ X &= t\phi/\omega^2, \end{aligned} \tag{A13}$$

with t_n for $n = 1, 2, 3, 4$ defined by

$$t_n = \tfrac{1}{2}(n-1)!\,\Omega^{n+1}[(1-\lambda)^{-n} - (-1-\lambda)^{-n}], \tag{A14}$$

and

$$\begin{aligned} \Omega &= \omega/\phi, \\ \omega &= \bar{\zeta} - \tfrac{1}{2}\lambda\bar{\alpha}, \\ \phi &= \tfrac{1}{2}[(1+\lambda)^{-1} + (1-\lambda)^{-1} - \bar{\alpha}]. \end{aligned} \tag{A15}$$

It is straightforward to eliminate R and X from the set of equations (A12) so as to obtain

$$\begin{aligned} 9t^2(v - w^2) + 20tw(u + w^2) + 10(1 - w)(u^2 + w^3) \\ = 20w^{3/2}[u(w - 1 - t) - wt]. \end{aligned} \tag{A16}$$

This equation is solved numerically for Ω for a fixed value of λ. The solution fixes the values of w, t, u, and v, and inserting these in (A12) yields R (and thus r) and X. From X and Ω one can compute ϕ and ω, and from these $\bar{\alpha}$ and $\bar{\zeta}$, and thus $\bar{c}$ and $\bar{a} - \bar{b}$. Finally, (A6) for $m = 2$ is equivalent to

$$2\eta r = 1 + R + 2\lambda\bar{\zeta} - \tfrac{1}{2}\lambda^2\bar{\alpha} - \omega^2/\phi, \tag{A17}$$

which determines η and, by (A4), $\bar{a} + \bar{b}$. The value of Δ may be obtained from (A5). Consequently, tricritical points may be generated parametrically by choosing a value of λ, solving (A16), and calculating the corresponding values of r, $\bar{a}$, $\bar{b}$, and $\bar{c}$. There may, of course, be more than one solution to (A16) for a given λ.

---

*Research supported by the National Science Foundation Grant GH-40285.

†Present address: Reactor Research Centre, Kalpakkam 603102, Tamil Nadu, India.

[1]J. L. Meijering, Philips Res. Rep. 5, 333 (1950); 6, 183 (1951).

[2]J. L. Meijering, Philips Res. Rep. 18, 318 (1963).

[3]M. Blume, Phys. Rev. 141, 517 (1966).

[4]H. W. Capel, Physica 32, 966 (1966); 33, 295 (1967).

[5]M. Blume, V. J. Emery, and R. B. Griffiths, Phys. Rev. A 4, 1071 (1971).

[6]J. Bernasconi and F. Rys, Phys. Rev. B 4, 3045 (1971).

[7]D. Mukamel and M. Blume, Phys. Rev. A 10, 610 (1974).

[8]S. Krinsky and D. Mukamel, Phys. Rev. B 11, 399 (1975).

[9]S. Krinsky and D. Mukamel, Phys. Rev. B 12, 211 (1975).

[10]J. Lajzerowicz and J. Sivardière, Phys. Rev. A 11, 2079 (1975); J. Sivardière and J. Lajzerowicz, *ibid.* 11, 2090 (1975); 11, 2101 (1975).

[11]R. L. Scott and P. H. Van Konynenburg, Discuss. Faraday Soc. 49, 87 (1970).

[12]R. B. Griffiths, Phys. Rev. B 12, 345 (1975).

[13]R. B. Griffiths and J. C. Wheeler, Phys. Rev. A 2, 1047 (1970).

[14]This list does not include all conceivable possibilities, but is restricted to those we have found in the three-component model.

[15]R. B. Griffiths, J. Chem. Phys. 60, 195 (1974).

[16]R. J. Baxter, J. Phys. C 6, L445 (1973); J. P. Straley and M. E. Fisher, J. Phys. A 6, 1310 (1973).

[17]See, J. M. Kincaid and E. G. D. Cohen, Phys. Rep. 22C, 57 (1975), p. 85.